

SYNTHESIS, CHARACTERIZATION AND CATALYTIC INVESTIGATION
OF IRON BASED NANO-CATALYTS FOR WATER OXIDATION REACTION

A THESIS SUBMITTED TO
THE GRADUATE SCHOOL OF NATURAL AND APPLIED SCIENCES
OF
MIDDLE EAST TECHNICAL UNIVERSITY

BY
SERRA KOCABAŞ

IN PARTIAL FULFILLMENT OF THE REQUIREMENTS
FOR
THE DEGREE OF MASTER OF SCIENCE
IN
CHEMISTRY

FEBRUARY 2022

Approval of the thesis:

**SYNTHESIS, CHARACTERIZATION AND CATALYTIC
INVESTIGATION OF IRON BASED NANO-CATALYTS FOR WATER
OXIDATION REACTION**

submitted by **SERRA KOCABAŞ** in partial fulfillment of the requirements for the degree of **Master of Science in Chemistry, Middle East Technical University** by,

Prof. Dr. Halil Kalıpçılar
Dean, Graduate School of **Natural and Applied Sciences**

Prof. Dr. Özdemir Doğan
Head of the Department, **Chemistry**

Prof. Dr. Emren Nalbant
Supervisor, **Chemistry**

Examining Committee Members:

Prof. Dr. Ceyhan Kayran
Chemistry, METU

Prof. Dr. Emren Nalbant
Chemistry, METU

Prof. Dr. Ayşen Yılmaz
Chemistry, METU

Prof. Dr. İrem Erel Göktepe
Chemistry, METU

Assoc. Prof. Dr. Oktay Demircan
Chemistry, Boğaziçi University

Date: 11.02.2022

I hereby declare that all information in this document has been obtained and presented in accordance with academic rules and ethical conduct. I also declare that, as required by these rules and conduct, I have fully cited and referenced all material and results that are not original to this work.

Name, Last name: Serra Kocabaş

Signature:

ABSTRACT

SYNTHESIS, CHARACTERIZATION AND CATALYTIC INVESTIGATION OF IRON BASED NANO-CATALYTS FOR WATER OXIDATION REACTION

Kocabaş, Serra
Master of Science, Chemistry
Supervisor: Prof. Dr. Emren Nalbant Esentürk

February 2022, 55 pages

The search for new energy storage technologies drew attention to the production of hydrogen from clean, renewable sources such as water with increase of scarcity of fossil fuels. Hence, water splitting electrochemically has been the centre of attention in recent years. However, water oxidation (oxygen evolution) (OER) reaction requires high potential to achieve large energy barrier occurred while transferring four electrons and four protons. To overcome this energy barrier, catalyst with high stability and activity can be used. For this, the earth-abundant metal oxide nanoparticles with high surface area and large numbers of active sites have gained great attention in literature. This thesis study aims to synthesize chromium-iron based metal oxide nanoparticles and to characterize synthesized nanomaterials via Scanning Electron Microscope (SEM), Transmission Electron Microscopy (TEM), X-Ray Photoelectron Spectrometry (XPS), X-Ray Diffraction (XRD), X-Ray Energy Dispersive Spectroscopy (EDX) and Brunauer-Teller-Emmett Isotherm (BET) techniques. The microscopy results showed that CrFeO_3 nanowires were formed by assembly of ca. 14 nm nanocrystallites. Electrocatalytic investigation of

the OER catalyst were studied in alkaline medium. To compare the activity of the nanocatalyst, benchmark RuO₂ used. CrFeO₃-FTO nanowires presented promising electrocatalytic performance with an onset potential of 1.63 V vs RHE at where RuO₂ had an onset potential of 1.47 V vs RHE, overpotential of 737 mV at 10 mA cm⁻² current density and Tafel slope of 57 mV dec⁻¹. As a result, CrFeO₃ nanomaterial was observed as comparable to that of RuO₂ and better than some iron-based metal oxide nanoparticles.

Keywords: Metal Oxide Nanoparticles, Nanocatalyst, Electrochemical Water Splitting, Oxygen Evolution Reaction

ÖZ

SPINEL YAPIDA NANO-KATALİZÖRLERİN SENTEZİ, KARAKTERİZASYONU VE SUYUN YÜKSELTGENMESİNDEKİ KATALİTİK ETKİNLİKLERİNİN İNCELENMESİ.

Kocabaş, Serra
Yüksek Lisans, Kimya
Tez Yöneticisi: Prof. Dr. Emren Nalbant Esentürk

Şubat 2022, 55 sayfa

Fosil yakıtların azalmasıyla birlikte yeni enerji depolama teknolojileri arayışı su gibi temiz, yenilenebilir kaynaklardan hidrojen üretimine yönelmiştir. Bu nedenle son yıllarda elektrokimyasal olarak suyun ayrılması ilgi odağı olmuştur. Ancak, suyun yükseltgenme tepkimesi dört elektron ve dört proton transferinden kaynaklanan büyük enerji bariyerine ulaşmak için yüksek potansiyele ihtiyaç duyar. Bu enerji bariyerini aşmak için yüksek kararlılık ve etkinliğe sahip katalizörler kullanılabilir. Yüksek yüzey alanına ve çok sayıda aktif bölgeye sahip metal oksit nanoparçacıklar literatürde büyük ilgi görmüştür. Bu tez çalışması, krom demir metal oksit nanoparçacıklarını sentezlemeyi ve sentezlenen nanomalzemeleri SEM, TEM, XPS, XRD, EDX ve BET teknikleri ile karakterize etmeyi amaçlamaktadır. Mikroskopi analizleri CrFeO₃ nanotellerinin yaklaşık 14 nm boyutundaki nanokristallerin bir araya gelmesiyle oluştuğunu göstermiştir. Katalizörün elektrokatalitik incelemesi alkali ortamda çalışılmıştır. Nanokatalizörün aktivitesini karşılaştırmak için RuO₂ kullanılmıştır. CrFeO₃-FTO nanotellerinin başlangıç potansiyeli 1.63 V vs RHE olarak hesaplanırken RuO₂ nanoparçacıklarının başlangıç potansiyeli 1.47 V vs RHE olarak, aşırı potansiyeli 10 mA cm⁻² akım yoğunluğunda 737 mV olarak ve Tafel

eđimi 57 mV dec^{-1} olarak görölmüştür. Katalizörün elektrokatalitik incelemesi alkali ortamda çalışılmıştır. Nanokatalizörün aktivitesini karşılaştırmak için RuO_2 kullanılmıştır. Sonuç olarak, CrFeO_3 nanomateryalinin RuO_2 ile kıyaslanabilir ve bazı demir bazlı metal oksit nanoparçacıklardan daha iyi olduđu gözlenmiştir.

Anahtar Kelimeler: Metal Oksit Nanoparçacık, Nanokatalizör, Suyun Elektrokimyasal Ayrıştırılması, Oksijen Salınımı Tepkimesi

To my love and my family,

ACKNOWLEDGMENTS

I would like to thank to my supervisor Prof. Dr. Emren Nalbant Esentürk for her endless encouragement, kindness, and support when I lost my hope during my master period. I am very glad to work with her.

I would like to express my sincere thanks to Dr. Asude Çetin for her mentorship over the past five years.

I acknowledge Prof. Dr. Ahmet Muhtar Önal for his guidance during electrochemical studies.

I thank Prof. Dr. Ayşen Yılmaz for access to XRD instrument and her group members for their help during the measurements.

I would like to thank the Central Laboratory of METU for their help during the characterizations of my materials.

I would like to thank Scientific and Technological Research Council of Turkey (TUBITAK) for the financial support under Project No: 117Z384

I would like to thank specially to my dearest labmates Yağmur Ağcalı and İzel Aksoy for their friendship, support in every challenge of my lab period. And also, I would like to thank all NanoClusMate Research Group members.

I am greatly thankful to my dear friend Burcu Aksoy who is like sister to me for her endless support, kindness, being like a walking encyclopedia for my every single question. Whenever I need, she always succours to me.

I am also sincerely thankful to my dear friends Elif Serel Yılmaz and Naciye Özmen who are the most special people the department brought to me. Their support, advice, making me laugh and all the moments we have had so far are so precious to me.

Finally, my deepest appreciation is for my family especially my mom Nilgün and my husband Ali. I am very grateful to have such a strong, patient, warm-hearted mom. She is always there for me, and I promise that I will always there for her. For believing in me, for his love and support, I am deeply grateful to my love and dearest friend Ali. I consider myself as a very lucky person thanks to him.

TABLE OF CONTENTS

| | |
|---|-----|
| ABSTRACT | v |
| ÖZ..... | vii |
| ACKNOWLEDGMENTS | x |
| TABLE OF CONTENTS | xii |
| LIST OF TABLES | xiv |
| LIST OF FIGURES | xv |
| LIST OF ABBREVIATIONS | xvi |
| 1 INTRODUCTION AND MOTIVATION..... | 1 |
| 2 METAL OXIDE NANOPARTICLES | 5 |
| 2.1 Introduction to Metal Oxide Nanoparticles | 5 |
| 2.2 Types of Metal Oxide Nanoparticles | 6 |
| 2.2.1 Spinel..... | 6 |
| 2.2.2 Perovskite | 7 |
| 2.3 Synthesis of Metal Oxide Nanoparticles | 8 |
| 2.3.1 Sol-Gel Method | 9 |
| 2.3.2 Hydro/Solvothermal Method..... | 10 |
| 2.4 Characterization of Metal Oxide Nanoparticles | 11 |
| 3 WATER OXIDATION REACTION | 13 |
| 3.1 Types of Water Oxidation Reaction | 14 |
| 3.1.1 Chemical Water Oxidation Reaction..... | 14 |
| 3.1.2 Photoelectrochemical Water Oxidation Reaction | 14 |

| | | |
|-------|---|----|
| 3.1.3 | Electrochemical Water Oxidation Reaction..... | 15 |
| 3.1.4 | Electrochemical Water Oxidation Reaction Mechanism..... | 16 |
| 3.2 | Electrochemical Characterization of an Electrocatalyst..... | 16 |
| 4 | EXPERIMENTAL..... | 19 |
| 4.1 | Materials..... | 19 |
| 4.2 | Synthesis of CrFeO ₃ Nanowires..... | 19 |
| 4.2.1 | Via Hydro/Solvothermal Method..... | 19 |
| 4.3 | Material Characterization..... | 20 |
| 4.4 | Electrochemical Characterization..... | 20 |
| 4.4.1 | Electrode Preparation..... | 20 |
| 4.4.2 | Electrochemical Measurements..... | 21 |
| 5 | RESULTS AND DISCUSSION..... | 25 |
| 5.1 | Characterizations of CrFeO ₃ Nanowires..... | 25 |
| 5.2 | Electrocatalytic Performance of CrFeO ₃ Nanowires..... | 32 |
| 6 | CONCLUSION..... | 43 |
| | REFERENCES..... | 45 |
| | APPENDICES..... | 55 |
| A. | Characterizations of CrFeO ₃ Nanowires at 550 °C Calcination Temperature..... | 55 |
| B. | Characterizations of CrFeO ₃ Nanowires at 650 °C Calcination Temperature..... | 55 |

LIST OF TABLES

TABLES

| | |
|--|----|
| Table 5.1 Summary of some recently reported representative OER electrocatalysts in alkaline medium together with the data obtained for CrFeO ₃ nanowires..... | 36 |
| Table 5.2 Change in the onset potential and overpotential (at 10 mA cm ⁻²) of CrFeO ₃ nanowires after constant potential electrolysis..... | 40 |

LIST OF FIGURES

FIGURES

| | |
|--|----|
| Figure 2.1 Spinel structure unit cell | 6 |
| Figure 3.1 Water oxidation reaction mechanism in basic medium..... | 16 |
| Figure 3.2 Illustration of onset potential determination..... | 17 |
| Figure 4.1. Schematic representation of preparation of the modified electrode | 21 |
| Figure 4.2. Schematic representation of the three-electrode system used for electrochemical measurements | 22 |
| Figure 4.3. Schematic representation of a Hoffmann electrolysis apparatus..... | 24 |
| Figure 5.1 (a) SEM image, (b)-(d) TEM images (at different magnifications) and SAED pattern (inset) and (e) elemental mapping (Cr (orange), Fe (green), O (red)) of CrFeO ₃ nanowires..... | 26 |
| Figure 5.2 EDX spectra of CrFeO ₃ nanowires..... | 27 |
| Figure 5.3 XRD Pattern of CrFeO ₃ nanowires (JCPDS card no: 01-075-9861) | 27 |
| Figure 5.4 XPS (a) survey, (b) Cr 2p, (c) Fe 2p, (d) O1s spectra of CrFeO ₃ nanowires | 31 |
| Figure 5.5 N ₂ adsorption isotherm of CrFeO ₃ nanowires | 32 |
| Figure 5.6 (a) Polarization curves of bare FTO, CrFeO ₃ nanowires and RuO ₂ in 0.1 M KOH at a scan rate of 5 mV s ⁻¹ (b) Tafel slope of CrFeO ₃ and RuO ₂ | 34 |
| Figure 5.7 Current density changes during controlled potential electrolysis in 0.1 M KOH and Polarization curves of CrFeO ₃ nanowires obtained before and after electrolysis at overpotential corresponding to initial current density of (a)-(b) j = 5 mA cm ⁻² and (c)-(d) j = 10 mA cm ⁻² | 39 |
| Figure 5.8 Nyquist plot for the CrFeO ₃ nanowires modified FTO electrodes at different overpotentials | 41 |
| Figure 5.9 Plot for change in the volume of O ₂ during the OER using the CrFeO ₃ - FTO in 0.1 M KOH..... | 42 |

LIST OF ABBREVIATIONS

ABBREVIATIONS

| | |
|----------------|---|
| OER | Oxygen Evolution Reaction |
| RHE | Reversible Hydrogen Electrode |
| XRD | X- Ray Diffraction |
| SEM | Scanning Electron Microscopy |
| EDX | Energy Dispersive X-Ray |
| TEM | Transmission Electron Microscopy |
| HR-TEM | High Resolution TEM |
| XPS | X-Ray Photoelectron Spectroscopy |
| ICP-OES | Inductively Coupled Optical Emission Spectroscopy |
| BET | Braunauer-Emmett-Teller |
| IR | Infrared Spectroscopy |
| LSV | Linear Sweep Voltammetry |
| EIS | Electrochemical Impedance Spectroscopy |
| FTO | Fluorine-doped Tin Oxide |
| CPE | Constant Phase Element |
| NTA | Nitrilotriacetic acid |
| PEO | Polyethylene oxide |
| FTIR | Fourier Transform Infrared Spectroscopy |
| TPR | Temperature Programmed Reduction |
| STEM | Scanning Transmission Electron Microscopy |
| MONP | Metal Oxide Nanoparticle |
| CE | Counter Electrode |
| WE | Working Electrode |
| HER | Hydrogen Evolution Reaction |
| ORR | Oxygen Reduction Reaction |

CHAPTER 1

INTRODUCTION AND MOTIVATION

Due to depletion of fossil fuels and their extensive usage in all over the world, the quest for renewable, clean, and sustainable energy source has been arisen. In this context, hydrogen has become centre of attention as an energy carrier. It can be obtained from water which is renewable and proper energy sources.

Electrochemically water splitting is an effective and easy way to produce hydrogen. However, water oxidation step occurring in anode (oxygen evolution reaction (OER)) is both thermodynamically and kinetically a demanding process due to high energy requisite for multiple electrons and protons transfers.¹ To overcome consisted energy barrier, overpotential is applied. On condition that the applied overpotential is reduced, the energy needed for the reaction cannot be achieved. Therefore, reducing the overpotential and enhancing reaction rate is critical problem. The use of suitable catalysts can be a very appropriate way to solve this problem.¹ The new catalyst system which demonstrates high stability and multiple application performance at low overpotential is vitally important. Thus, researchers have been focused on designing and producing new metal-oxide nanoparticles as effective electrocatalysts for water oxidation reaction.

To improve OER, RuO₂ and IrO₂ metal oxides have been reported as the most efficient electrocatalysts. Although RuO₂ and IrO₂ are very effective electrocatalysts for water oxidation reaction, their high cost and low stability under alkaline conditions lead researchers to explore new water oxidation catalysts with high catalytic activity and low cost.²⁻⁵ As the result of these research, metal oxide

electrocatalysts which are produced from cheap and earth-abundant metals have great potential with their high stability and electrochemical activity.

Bimetallic metal oxide catalysts such as spinel, perovskite have great attention due to their multiple valence state, endurance for catalysis and activity in alkaline medium.⁶⁻¹³ Also, these electrocatalysts are made of several earth abundant metals. These compositions are comparable to those of high-cost metal oxide catalysts.

Among earth abundant transition metals, iron based multimetallic oxides have a great attention due to their high electrical conductivity, availability and producibility with ease, and magnetic property.^{2,3,22-30,14-21} Liu et al. has been examined NiFe₂O₄ spinel nanorods as a catalyst for oxygen evolution reaction. For comparison, different temperature has been used for synthesis of material through the same procedure. At 350 °C, the synthesized nanomaterial has showed the most enhanced catalytic activity. Overpotential at 10 mA/cm⁻² was found as 342 mV, and Tafel slope has been detected as 44 mV dec⁻¹.² Another study of iron substituted metal oxide catalyst is the synthesis of CuFe₂O₄ crystals for water oxidation reaction by Liu et al. In the study, RuO₂ has been used to compare the activity of the nanomaterial. As a water oxidation catalyst, CuFe₂O₄ nanomaterials has showed 2.2 times higher performance than commercial RuO₂ during the process. Tafel slope of synthesized material has been found as ~52 mV dec⁻¹ while the commercial one was ca. 49 mV dec⁻¹.³¹ Yuan et al. have investigated the tubular ferrite MFe₂O₄ (M=Fe, Co, Ni) microstructures for water splitting. For the comparison of electrochemical activities of these materials, overpotential has been used. The results were 340, 392 and 432 mV for NiFe₂O₄, CoFe₂O₄ and Fe₃O₄ respectively. Among the results, NiFe₂O₄ has been reported as the most effective combination of the study.³²

Combination of iron based mixed metal oxides and chromium metal has gained great attention and have been investigated for their structural, magnetic and electronic properties in the last decades.^{14,15,34,35,16-18,24-26,29,33} For instance, Banerjee et al. have studied on Cr/Fe oxide samples for catalytic decomposition of sulfuric acid. In the

study, $\text{Fe}_{1.8}\text{Cr}_{0.2}\text{O}_3$ mixed metal oxide catalyst has been synthesized and its characterization has been carried out with XRD and FT-IR for the decomposition reaction.¹⁴ Freire et al. have reported a structural study of a new electroceramic composite $\text{Pb}(\text{Fe}_{0.5}\text{Nb}_{0.5})\text{O}_3$ (PFN)- $\text{Cr}_{0.75}\text{Fe}_{1.25}\text{O}_3$ (CRFO).¹⁵ Rocha et al. have also worked with Cr-Fe oxides ceramic composites with CaTiO_3 for their thermal stability, structural and dielectric properties in microwave region.¹⁶ Another study of Cr-Fe containing ceramic composite has been worked by de Araujo et al. In the study, the activity of iron containing ceramic composites (Fe, Cu, Cr, Pb and/or Ti) for dehydrogenation of ethylbenzene in the presence of CO_2 has been examined. Ceramic composites consisted of one of the Cr-Fe oxides which is $\text{Cr}_{0.75}\text{Fe}_{1.25}\text{O}_3$ in trigonal structure. After characterizations, TPR curves showed that Cr stabilizes Fe^{3+} in $\text{Cr}_{0.75}\text{Fe}_{1.25}\text{O}_3$ matrix. The catalytic activity of $\text{Cr}_{0.75}\text{Fe}_{1.25}\text{O}_3$ has been investigated, and high activity of the multimetallic oxides has been observed.¹⁷ In the report of Ozkendir, the electronic and structural properties of FeCrO_3 sample have been studied. To compare the data, Cr_2O_3 and $\alpha\text{-Fe}_2\text{O}_3$ has been used.¹⁸ Kanazawa and Maeda have been investigated Cr-Fe mixed oxide powder as a catalytic material for photochemical and electrochemical water oxidation reaction. Under both electrochemical and photochemical conditions, the activity of Fe-Cr mixed oxides has been found lower than the one of Fe_2O_3 . This is mostly because oxidation of Cr^{3+} ions on the surface has been lowered the surface activity. Substitution of Cr^{3+} ions in Fe_2O_3 has increased charge transfer in the bulk material, thereby the overall reaction has been enhanced.²⁴ Benhalima et al. have studied the structural, electronic and magnetic properties of CrFe_2O_4 and FeCr_2O_4 as theoretically. To investigate these properties, density functional theory (DFT) using spin polarized calculations with generalized gradient approximation (GGA-PBE) has been used.³³ Ghoneim et al. have been investigated the structural, thermal and electrochemical studies of $\text{CrSm}_x\text{Fe}_{1-x}\text{O}_3$ nanoperovskite ($x = 0, 0.035, 0.07, 0.1$ and 0.15). The nanomaterial has been prepared with auto-compassion strategy. The nanoperovskite has been exhibited a promising electrochemical activity as an electrode for energy storage application.³⁴ Mubasher et al. have been examined

multi-walled carbon nanotubes and CrFe_2O_4 nanoparticles nanohybrids as an anode materials for lithium-ion batteries. These MWCNT/ CrFe_2O_4 nanohybrids presented high efficiency, and low-cost and eco-friendly production of metal oxides-based anode materials for lithium-ion batteries.³⁵ Yet, to the best of our knowledge there has been no report on synthesis of Cr-Fe multimetallic oxide structure in wire morphology and their electrocatalytic investigation in OER before this study.

The aim of this thesis study is to synthesize chromium substituted iron oxide nanowires for catalytic application in water oxidation reaction. Hydrothermal method in which nitrilotriacetic acid was used as a surfactant was performed to synthesize the nanomaterials. Synthesized nanomaterials were characterized by different analytical techniques. After characterization, it was observed that spherical-like CrFeO_3 nanoparticles assembled to form nanowires with a length in micron range. To investigate the performance of the catalyst in water oxidation, the fluorinated tin oxide (FTO) glass substrates were modified with synthesized nanomaterials. The results showed that CrFeO_3 can be considered as efficient, durable, cost-effective electrocatalyst.¹⁰

CHAPTER 2

METAL OXIDE NANOPARTICLES

2.1 Introduction to Metal Oxide Nanoparticles

Metal oxide nanoparticles (MONPs) have numerous application areas in chemistry, physics and materials science. They can be used as conductive materials, sensors and catalysts in aforementioned areas. Unique properties of oxide nanoparticles are supplied by their limited size and edge surface sites as high density. Nanoparticle size of oxide material enhance three basic properties. First one is structural characteristic of material, also known as cell parameters or lattice symmetry. For instance, CuO, ZnO, TiO₂, etc. are some nanoparticles in which cell parameters change due to the alterations of structure size. As decreasing the size of nanoparticles, an increase in surface free energy and stress can be observed on the material surfaces. To stabilize the material as structural, low surface free energy must be achieved. Secondly, nanoparticle size and shape can influence the magnetic properties of the nanomaterial. As an example, γ -Fe₂O₃ nanoparticles have size dependent magnetic properties where ferromagnetic behaviour is observed at 55 nm particle size while 12 nm nanoparticles show superparamagnetic behaviour. Another size dependent property of a metal oxide nanoparticle is electrical one. In bulk oxides, wide band gaps and low reactivity are observed. Decreasing the average size of an oxide particle causes changes in the band gap which is related to the conductivity and reactivity of the metal oxide nanoparticles.^{36,37}

2.2 Types of Metal Oxide Nanoparticles

Metal oxide structures consist of large oxide ions in cubic or hexagonal- packed arrays and metal cations occupying the holes formed by octahedral or tetrahedral networks. Structure of a MONP can be detected as many different types which are rock salt, wurtzite, rutile, perovskite, spinel and corundum-type. Two of the most commonly studied one; spinel and perovskite are described in the following sections.

2.2.1 Spinel

General spinel forms can be described as AB_2O_4 , where A and B are metal ions in different oxidation states. For normal spinels, metal A cations occupy one-eighth tetrahedral holes, metal B cations occupy half the octahedral holes while O^{2-} anions arrange in a cubic close-packed lattice. (Figure 2.1) To retain the valence equilibrium, cation A has oxidation states of +2 or +4 while cation B has oxidation states of +3 or +2, respectively. ($A^{2+}B_2^{3+}O_4^{2-}$ or $A^{4+}B_2^{2+}O_4^{2-}$) For the formation of a spinel structure, commonly used metals for A sites are Li^+ , Mg, Ca, Ba, Mn, Fe, Co, Cu etc. while for B site, Cr, Mn, Fe, Co, Ni etc. Also, some other spinel forms such as sulfide, selenide, nitride etc. are examined in literature. ⁸

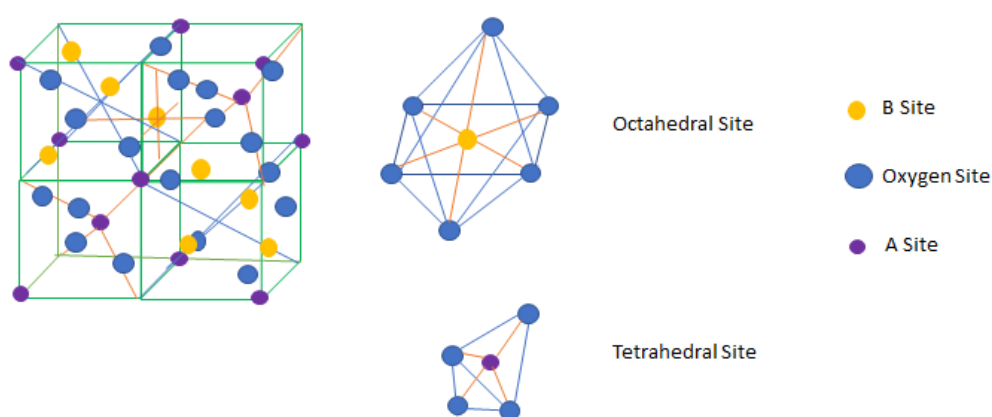


Figure 2.1 Spinel structure unit cell

There are three types of spinel structures which are normal, inverse and complex spinels. These classifications have been done by considering A and B distributions in tetrahedral and octahedral holes. Normal spinel structure was examined above. Inverse spinel structure can be described as the formula of $B(AB)O_4$. In this structure, all of the A cations and half of the B cations occupy octahedral holes while the other half of the B cations occupy tetrahedral holes. $NiFe_2O_4$ can be a good example for inverse spinel structure. According to distributions of Ni and Fe ions, the structure of the sample can be represented as $Fe(NiFe)O_4$. In complex spinels, both A and B metal ions are distributed through the tetrahedral and octahedral holes as mixed. For instance, in $CuAl_2O_4$ spinel structure, Cu^{2+} and Al^{3+} cations occupy the octahedral and tetrahedral holes partially.⁸

2.2.2 Perovskite

Perovskite structures are formulated as BAO_3 where B cation which occupies twelve-fold coordination site is located at the centre of the cube, and A-site cations which occupy six-fold coordination site are located at the eight corners of the cube. Oxide ions are located on the centres of 12 edges.³⁸ (Figure 2.2)

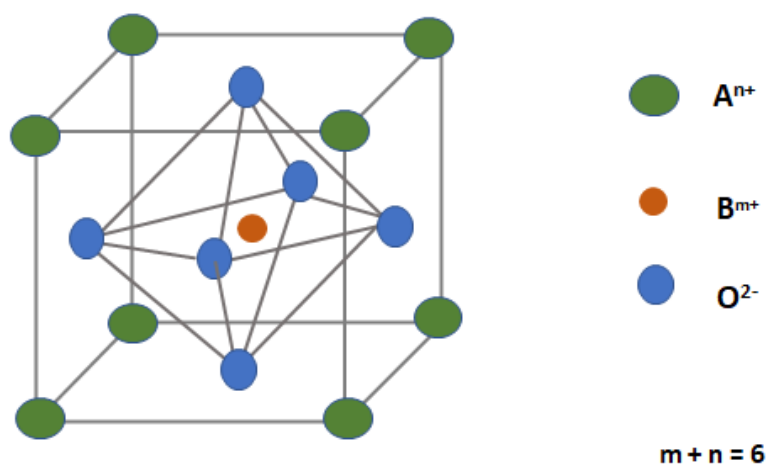


Figure 2.2 Perovskite unit cell

The charge distributions in perovskite structure can be presented as three different formulations which are $A^{2+}B^{4+}O_3^{2-}$, or 2:4 perovskites; $A^{3+}B^{3+}O_3^{2-}$, or 3:3 perovskites; and $A^+B^{5+}O_3^{2-}$, or 1:5 perovskites.

2.3 Synthesis of Metal Oxide Nanoparticles

Due to their numerous properties and several application areas, metal oxide materials at the nanoscale have gained great attention in nanotechnology. Therefore, researchers give priority to explore new synthetic methods to prepare these materials. After countless research so far, many different approaches to obtain nanomaterials in different compositions and crystal structures have been detected. These different approaches can be categorized under two basic topic which are top-down and bottom-up. Top-down approach consists of physical methods while bottom-up approach contains both physical and chemical methods. (Figure 2.3)

Top- down approaches are related with the process of nanoscale structure formation from macroscopic structures by using lithography or related techniques. However, this method has some limitations such as its high cost, unrepeatable process, formations of irregular features in atomic scale and uncontrolled particle size. On the contrary, bottom-up methods perform the miniaturization of large-scale material to atomic level by using specific and non-covalent interaction between molecules to assemble different nanoscale structures. Moreover, the use of atoms, molecules or nanoparticles as building blocks ensure the crystallite size and/or shape control. The bottom-up approach consists of many different methods which are basically collected under the name of solid-phase, solution-phase and vapor-phase.³⁹

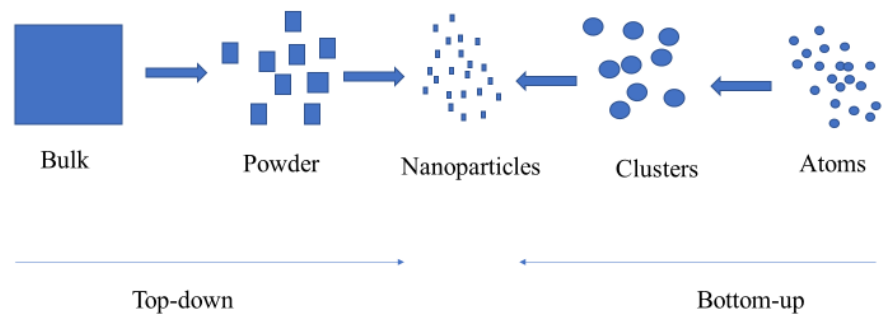


Figure 2.3 Schematic representation of top-down and bottom-up approaches

Among all methods, solution-phase synthesis become prominent through solid-phase and gas-phase. The method is controlled over reaction pathways, and different crystal structure of nanomaterial can be synthesized. Also, size distribution as uniform and homogeneous compositions are achieved by the method. Sol-gel method and hydro/solvothermal method are commonly used methods for the synthesis of metal oxide nanoparticles in solution-phase category.³⁹

2.3.1 Sol-Gel Method

Sol-gel process is frequently used method for the synthesis of metal oxide nanoparticles. The method requires low calcination temperature, cost-efficient precursors, and simple set-up for the synthesis. The method leads to the production of metal oxide nanoparticles in good size distribution and high yield and purity.

In the sol-gel process, the metal oxide nanoparticles are synthesized with four steps of 1) procuring homogeneous aqueous solution, 2) water evaporation, 3) drying the gel at a fixed temperature, and 4) calcination.⁴⁰ (Figure 2.4)

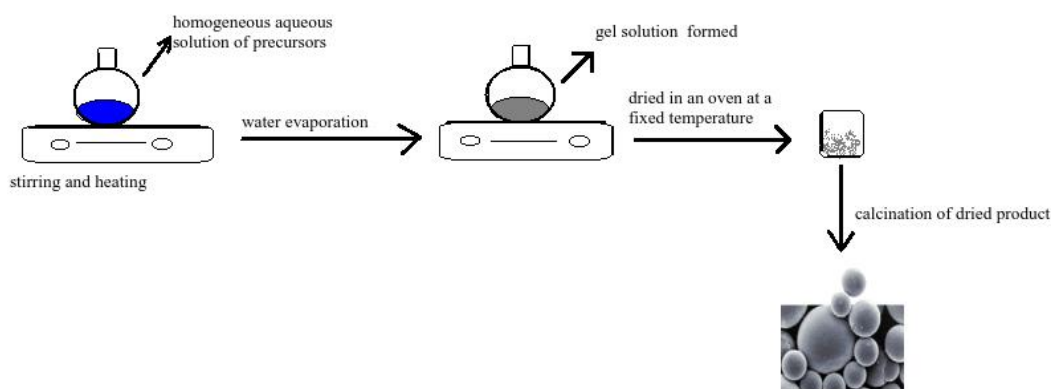


Figure 2.4 Sol-gel process illustration

2.3.2 Hydro/Solvothermal Method

In hydro/solvothermal method, chemical reactions occur in a closed vessel at higher temperature than the boiling point of the solvent used.³⁹ When employed solvent is water, method is defined as hydrothermal. In solvothermal method, different solvents other than water such as ethanol, isopropanol etc. can be used. In hydro/solvothermal method, autoclaves can be utilized as reaction vessels due to their high temperature and pressure endurance.

In the process, metal precursors are dissolved in the solvent, and then the mixture is heated in the autoclave. In the heating process, regions occur with two different temperatures. In hotter region, the precursors are dissolved and settled at the bottom of vessel. This saturated solution is transported to upper part while the cooler and denser part of the solution descends to the vessel. As reducing the temperature in the upper part, solution becomes supersaturated and crystal formation occurs at the bottom.⁴¹ (Figure 2.5)

By using this method, desirable nanomaterials with controlled shape and size can be obtained by the modifications on temperature, solvent, and surfactants. Surfactants

such as nitrilotriacetic acid (NTA), urea, citric acid etc. help to modify nanomaterial morphology.⁸

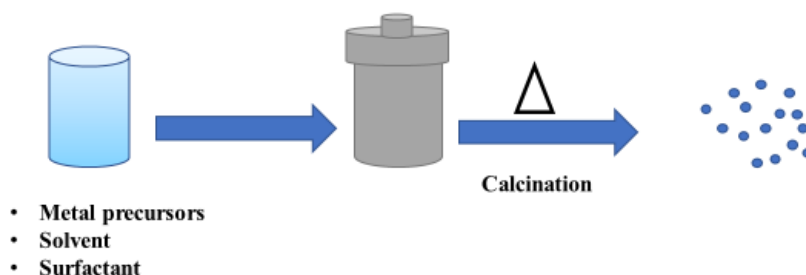


Figure 2.5 Schematic representation of hydro/solvothermal method

2.4 Characterization of Metal Oxide Nanoparticles

After the synthesis of metal oxide nanoparticles, it is important to enlighten their properties. To characterize materials, there are various techniques which help to analyze material as structural, morphological, and compositional.

Among the techniques, electron microscopy has a special importance due to its ability to detect surface topography, morphology, size and shape the nanomaterial. Scanning electron microscopy (SEM) performs surface topography analysis but this technique cannot give information on atomic scale because of its poor resolution. On the contrary, transmission electron microscope (TEM) informs about nanoparticle size, shape, and composition. In addition, by using high resolution TEM (HR-TEM), information about diffraction patterns and lattice imperfections in nanomaterials on an atomic resolution scale can be reached. Energy dispersive X-ray spectroscopy (EDX) is used with SEM and TEM to give basic elemental information of the nanoparticles.

The crystal structure of the nanoparticle is generally examined by X-ray diffraction analysis (XRD). The crystal structure of a material can be determined by analysing the X-ray pattern which gives the information about lattice space character.

Moreover, by using Debye-Scherrer equation, crystallite size of the material can be found. The equation where τ is crystallite size, κ is dimensionless shape factor, λ is wavelength of X-ray in nm, β is line broadening at full width half maximum and θ is the Bragg angle is shown below.⁴²

$$\tau = \frac{\kappa\lambda}{\beta \cos\theta} \quad (2.1)$$

To analyze surface properties of nanoparticles, X-ray photoelectron spectroscopy (XPS) can be used. Photoelectrons are emitted from the surface of nanoparticles which are irradiated by X-ray beam. These emitted photoelectrons have specific energy levels which help to discover the chemical state, and the overall electronic structure and the density of the electronic states in the material. Thus, one can obtain both quantitative and qualitative information about the surface structure of nanoparticles using XPS.

Brunauer-Emmett-Teller (BET) isotherm is an example for adsorption-desorption techniques in which pore volume, size of the nanomaterial and surface area can be examined.

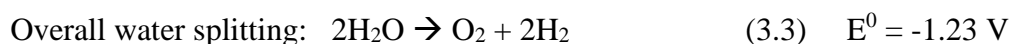
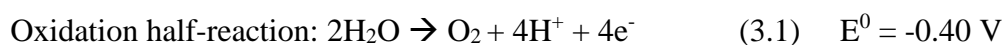
There are some other techniques such as infrared spectroscopy (IR), inductively coupled optical emission spectroscopy (ICP-OES), Raman spectroscopy etc. to perform further elemental analysis of nanoparticles.

CHAPTER 3

WATER OXIDATION REACTION

Because of extensive usage of fossil fuels which release greenhouse gases, energy crisis may emerge in the future. Hence, finding and improving new energy sources become the focus of researches. Contrary to fossil fuels, these new energy sources with renewable and sustainable features have gained great attention so far.²⁸ However, some pivotal problems considering new sources arise from the deficiency of reliable methods for energy storage.³² To cope with this problem, researches lead to find new method which is achieved to store the energy in chemical bonds of a proper fuel.⁴³

In this context, hydrogen has gained great attention due to high energy stored in its bonds. It can be obtained from readily available, abundant and renewable energy sources such as water via water splitting. The electrocatalytic water splitting is a well-used technique which produces hydrogen and oxygen. The reactions of the process are summarized in below.



However, the overall water splitting reaction, especially water oxidation, is a difficult process because of requiring high energy to occur.²⁰ To achieve the energy barrier of the reaction, a proper catalyst can be used. Photosystem II which is the biological water oxidation in plants (photosynthesis) is the mastermind of synthetic catalytic water oxidation. In the oxygen evolution center of photosystem II, Mn_4CaO_5 clusters act as a catalyst.²² By considering this cluster, researches have been focused on

synthesizing new, active and stable catalysts. In these intense researches, transition metals used for the formation of new catalyst systems have gained great attention.

3.1 Types of Water Oxidation Reaction

Water oxidation reactions can be examined under three main topic which are chemical, photochemical, and electrochemical.

3.1.1 Chemical Water Oxidation Reaction

As explained above, the structure of the Mn_4CaO_5 cluster of PSII has inspired the research for the generation of synthetic catalysts based on transition metal ions that oxidize water to oxygen. To activate a metal oxide catalyst in water oxidation, the use of sacrificial reagents such as sodium periodate ($NaIO_4$), hypochlorite (ClO^-) etc. is obliged. By using these chemical oxidants, a catalyst performs in a simple and fast way. However, catalyst activity is reduced and/or transformed catalyst to another material since these reagents are consumed during the reaction. As a result of this, catalyst stability and thus, experimental results get affected.⁴⁴

3.1.2 Photoelectrochemical Water Oxidation Reaction

In photochemically- driven water oxidation catalysis, light is used to activate the catalyst and then, oxidize water. There are three approaches to achieve the catalytic reaction. First one is three-component system which contains photosensitizer, a molecular water oxidation catalyst and a sacrificial electron acceptor such as $S_2O_8^{2-}$ or $[Co(NH_3)_5Cl]^{2+}$. As photosensitizer, $[Ru(bpy)_3]^{3+}$ and derivatives are the most used compounds due to their high redox potentials, long excited-state lifetime, and strong visible absorbance. Briefly, by absorbing light, photosensitizer gets excited and transfers electron to sacrificial electron acceptor. With oxidization of photosensitizer, catalyst is activated and thus, catalytic cycle is set off. The main

problem of this system is that stability of the photosensitizer is affected due to the reactivity of singlet oxygen formed during the photocatalysis.⁴⁴

The second approach is based on the usage of covalent dyad photosensitizer-water oxidation catalyst or triad photosensitizer-catalyst-photosensitizer multi-molecular assemblies. In this approach, two metal complexes covalently bound within same metal.

The final approach is the using semiconductor as photocatalyst while metal part of the composite is the co-catalyst.⁴⁵ As light with higher energy than its band gap contacts with semiconductor surface, an electron is transferred from the valence band of photocatalyst to conduction band and thus, an electron-hole pair is formed. Water absorbed on the positively charge holes and then, it is oxidized. At that point, reduction of protons by electrons occurs and they are transferred to the co-catalyst.

3.1.3 Electrochemical Water Oxidation Reaction

In the electrochemical water oxidation, catalysts are activated by the applied potential and water molecules are oxidized by these activated catalysts. By controlling the applied overpotential, this oxidation reaction seems as a promising system. However, high energy barrier which is occurred while breaking the H-O bonds and forming O-O bond is an obstacle for obtaining a high performance from the process. To overcome the energy barrier problem, it is very important to maintain catalyst performance while fastening the reaction. Therefore, to select a proper catalyst with high stability and low overpotential is essential.

3.1.4 Electrochemical Water Oxidation Reaction Mechanism

There are various mechanisms has been suggested for the water oxidation reaction in the presence of a catalyst. One of the most commonly reported mechanism of the reaction that occur in basic medium is given below. In this mechanism M indicate active metal surface and species such as -OH, -OOH and O₂ adsorb on metal surface.

8



Figure 3.1 Water oxidation reaction mechanism in basic medium

3.2 Electrochemical Characterization of an Electrocatalyst

To evaluate an electrocatalyst in water oxidation reaction, some parameters such as onset potential, overpotential, Tafel slope, capacitance, stability etc. are crucial. To obtain these electrochemical data, numerous electrochemical techniques are used. Some of these techniques are linear sweep voltammetry (LSV), electrochemical impedance spectroscopy (EIS), chronoamperometry, controlled potential coulometry etc.

Polarization curves can be examined by LSVs of applied electrode modified with inspected catalyst. After obtaining the polarization curves, it is possible to observe three main data about the activity of that catalyst. First data obtained is onset potential which helps to find starting potential of the water oxidation at a current density of $10 \mu\text{A cm}^{-2}$.⁸ The onset potential of the reaction can be also measured by the intersection point of tangent lines. One of the tangent lines is drawn at the faradaic region where there is an increase in current density while other one is drawn at non-faradaic region.⁴⁶ (Figure 3.1)

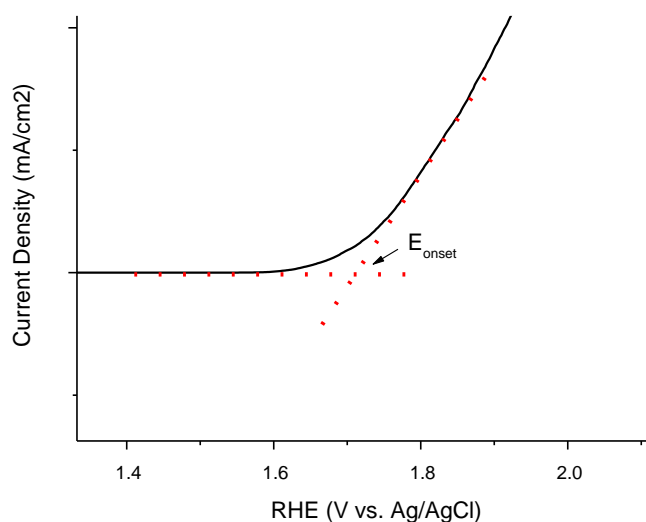


Figure 3.2 Illustration of onset potential determination

Another used parameter is overpotential which is defined as the potential difference between applied and equilibrium potentials. Normally, these two potentials should be equal but to reduce energy barrier, higher potential than equilibrium potential is applied.⁸ The equation is described to find overpotential is shown below. In the equation, E is applied potential, η is overpotential and E_{eq} is equilibrium potential.

$$\eta = E - E_{eq} \quad (3.4)$$

Tafel slope which gives information about reaction mechanism and the rate determining step of the overall reaction also helps to evaluate the catalytic activity

of the catalyst. By fitting the linear portion of polarization curves to Tafel equation (3.5), slope can be found. The equation of the Tafel slope where η is the overpotential and a, j and b are intercepts is shown below.⁸

$$\eta = a + b \log(j) \quad (3.5)$$

And finally, stability of an electrocatalyst can be examined via constant potential application to modified electrode for certain period of time. Observation of a possible change in current density in time, is an effective way to measure stability of the catalyst. No change in current density imply high stability of the electrocatalyst. By comparing polarizations curves with considering onset potentials, overpotentials and Tafel slopes before and after electrolysis, stability of the catalyst can be also examined.

CHAPTER 4

EXPERIMENTAL

4.1 Materials

All purchased chemicals were used as received without further purification. Chromium (III) nitrate nonahydrate ($\text{Cr}(\text{NO}_3)_3 \cdot 9\text{H}_2\text{O}$), iron (III) nitrate nonahydrate ($\text{Fe}(\text{NO}_3)_3 \cdot 9\text{H}_2\text{O}$), isopropyl alcohol, nitrilotriacetic acid (NTA), acetylacetone, polyethylene oxide (PEO) and Triton X were purchased from Sigma Aldrich. Deionized ultra-pure water (18 M Ω , PURELAB Option-Q, ELGA) was used in the preparation of aqueous solutions.

4.2 Synthesis of CrFeO_3 Nanowires

4.2.1 Via Hydro/Solvothermal Method

The synthesis of CrFeO_3 nanowires were carried out by using a previously reported hydrothermal method with some modifications.⁴⁷ In the synthesis, $\text{Cr}(\text{NO}_3)_3 \cdot 9\text{H}_2\text{O}$ (3.0 mmol), $\text{Fe}(\text{NO}_3)_3 \cdot 9\text{H}_2\text{O}$ (6.0 mmol) and NTA (4.7 mmol) were added to 30.0 mL isopropanol and 10 mL deionized ultra-pure water mixture at room temperature. The prepared solution was stirred vigorously until a homogeneous mixture was obtained. After complete dissolution, the mixture was transferred to a 100 mL Teflon lined stainless steel autoclave and heated to 180°C. The mixture in autoclave was kept at that temperature for 6 hours. The product of synthesis was collected from the solution by centrifugation as precipitate. The precipitate was washed with deionized ultra-pure water and ethanol for several times. After washing the precipitate, it was dried at 60 °C for 8 h. Finally, the dried product was calcined at 450 °C for 1 hours, and nanoparticles were obtained as reddish-brown powder.

The synthesis products were dried at different calcination temperatures such as 550 °C and 650 °C. The synthesized nanomaterials were characterized by SEM and XRD analysis. However, obtained results (see Appendices) showed that the desired material could not be obtained with these experimental parameters.

4.3 Material Characterization

FEI Nova Nano SEM 430 was used for performing scanning electron microscopy (SEM) images and energy-dispersive X-ray (EDX) analysis. The transmission electron microscopy (TEM), scanning TEM (STEM) measurements, and elemental composition analyses were carried out by using FEI Tecnai G2 F30 electron microscope operating at 300 kV). Rigaku Ultima IV X-ray diffractometer with Cu K α radiation ($\lambda = 1.54 \text{ \AA}$) was used for characterizing the nanomaterials' structure in the 2θ range from 10° to 80° . X-ray photoelectron spectroscopy (XPS) analyses were carried out on PHI-5000 Versa Probe [Physical Electronics (PHI) Chanhassen, Minneapolis, MN], equipped with Al K α at 1486.92 eV source. In this analysis, all data were calibrated to hydrocarbon contamination peak at C1s of 284.0 eV. Brunauer-Emmett-Teller (BET) analysis with Autosorb-6 (Quantachrome Corporation) instrument was used to determine specific surface areas of synthesized nanomaterials. For all samples, dehydration was done at 300 °C for 5 h before analysis.

4.4 Electrochemical Characterization

4.4.1 Electrode Preparation

Fluorine-doped tin oxide (FTO) glass substrates were used in this study to analyze electrochemical characteristics of CrFeO₃ nanowires, FTO glass substrates with 0.5 cm² surface area were modified according to a previously reported method.⁴⁸

Before coating process, FTO glass was cleaned in dilute H₂SO₄ solution by sonication for 30 min. Then, cleaned FTO glass was calcined at 400 °C for 30 min. After cleaning FTO glass, 100.0 mg of catalyst and 30.0 mg of PEO were added into the mixture of 100.0 μL of Triton-X, 100 μL of acetylacetone and 1.0 mL of deionized water. The obtained solution was stirred vigorously for 24 h. After a homogeneous solution was obtained, 5.5 μL of the solution was transferred onto FTO glass. The catalyst loading was calculated as ca. 0.92 mg cm⁻². Finally, the electrodes were dried at 60 °C for 1 h, and calcination was performed at 450 °C for 1 h. (Figure 4.1)

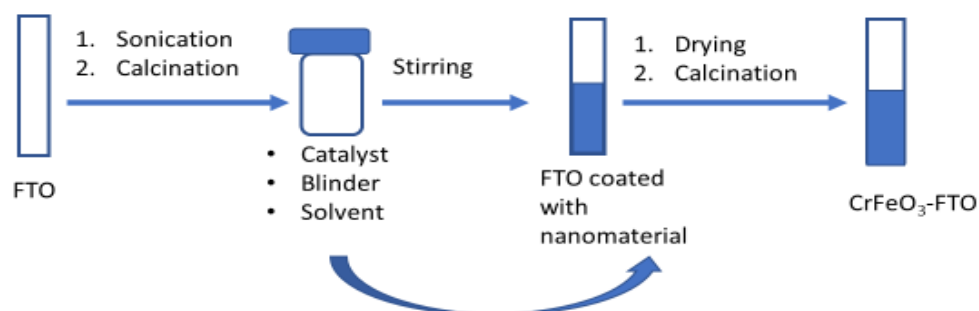


Figure 4.1. Schematic representation of preparation of the modified electrode

4.4.2 Electrochemical Measurements

Gamry 1010B potentiostat-galvanostat was applied for electrochemical measurements. All measurements were carried out at room temperature in a standard three-electrode system. (Figure 4.2) In this system, counter electrode (CE) was Pt wire and reference electrode was Ag/AgCl (in 3.0 M NaCl). FTO glass coated with CrFeO₃ nanomaterials were used as working electrodes (WE).

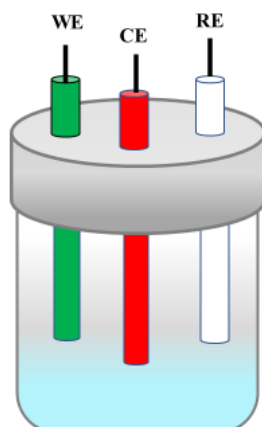


Figure 4.2. Schematic representation of the three-electrode system used for electrochemical measurements

FTO electrodes modified with CrFeO_3 nanomaterials were examined electrochemically in alkaline medium (0.1 M KOH solution). The polarization curves were set at a scan rate of 5 mV s^{-1} . All potentials were reported against reversible hydrogen electrode (RHE). The measured potential (vs. Ag/AgCl) was turned into RHE by using Nerst equation (4.1).⁸ Overpotential was calculated by using equation (4.2).

$$E_{\text{RHE}} = E_{\text{Ag/AgCl}} + E^{\circ}_{\text{Ag/AgCl}} + (0.059 \times \text{pH}) \quad (E^{\circ}_{\text{Ag/AgCl}} = 0.198 \text{ V}) \quad (4.1)$$

$$\eta = E_{\text{RHE}} - 1.23 \text{ V} \quad (4.2)$$

The linear part of polarization curves was fitted to Tafel equation for enlightening the kinetics of nanoparticles in water oxidation.

Constant potential electrolysis was used to examine the stability of the CrFeO_3 -FTO in alkaline medium of 0.1 M KOH. Overpotential of 585 mV for 10800 s, and 738 mV for 3600 s were obtained after the electrolysis. Electrochemical impedance spectroscopy (EIS) analysis was done at different potentials in the frequency range of 0.1 Hz – 100 kHz and with an amplitude of 20 mV.

The determination of mass activity ($A g^{-1}$) values was done by using the equation (4.3) at a certain overpotential.

$$\text{Mass activity} = j / m \quad (4.3)$$

where m ($mg cm^{-2}$) is the catalyst loading and j ($mA cm^{-2}$) is the current density.

Hoffmann electrolysis apparatus (Figure 4.3) was used to measure the volume of O_2 gas evolved during electrolysis at a constant current of 5 mA for 1 h. Thus water oxidation activity of FTO modified with $CrFeO_3$ nanowires were examined. Faradaic yield, described as the ratio between amounts of O_2 gas obtained experimentally to the theoretical one, was calculated. Theoretical amount of O_2 was calculated by using the following relations:

- I. Amounts of charges (Q) passing through the system was calculated by using Faraday's relation (4.5),

$$Q = i \cdot t \quad (4.4)$$

where i is the current (A) and t is time (s).

- II. Mole of O_2 ($n(O_2)$) was calculated by equation (4.5),

$$n(O_2) = Q / (n_e \cdot F) \quad (4.5)$$

where n_e is the mole of electrons passing the system for O_2 generation (4 moles) and F is the Faraday's constant ($96485 C mol^{-1}$).

- III. Theoretical volume of O_2 ($V(O_2)$) was calculated using ideal gas law (4.6),

$$P V(O_2) = n(O_2) RT \quad (4.6)$$

where P is atmospheric pressure which is 0.9 atm in Ankara, T is temperature (K) and R is the ideal gas constant ($0.082 L atm mol^{-1} K^{-1}$).

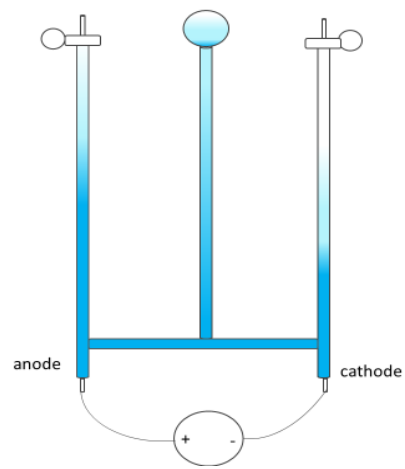


Figure 4.3. Schematic representation of a Hoffmann electrolysis apparatus

CHAPTER 5

RESULTS AND DISCUSSION

5.1 Characterizations of CrFeO₃ Nanowires

CrFeO₃ nanowires were synthesized via modified hydrothermal method based on a method previously described in the literature.⁷ Morphological character of CrFeO₃ nanowires were examined by SEM and TEM (Figure 5.1 a-d). The microscopy images show that nanoparticles with size of 14 nm ± 5 nm assemble to form nanowires (Figure 5.1 a,b). The existence of both Cr and Fe in the synthesized nanomaterials was proved by EDX analysis (Figure 5.2). The composition of CrFeO₃ was examined by the elemental mapping of Cr, Fe and O on nanowires (Figure 5.1e). The elemental mapping show that these elements are homogeneously distributed through the whole nanomaterial.

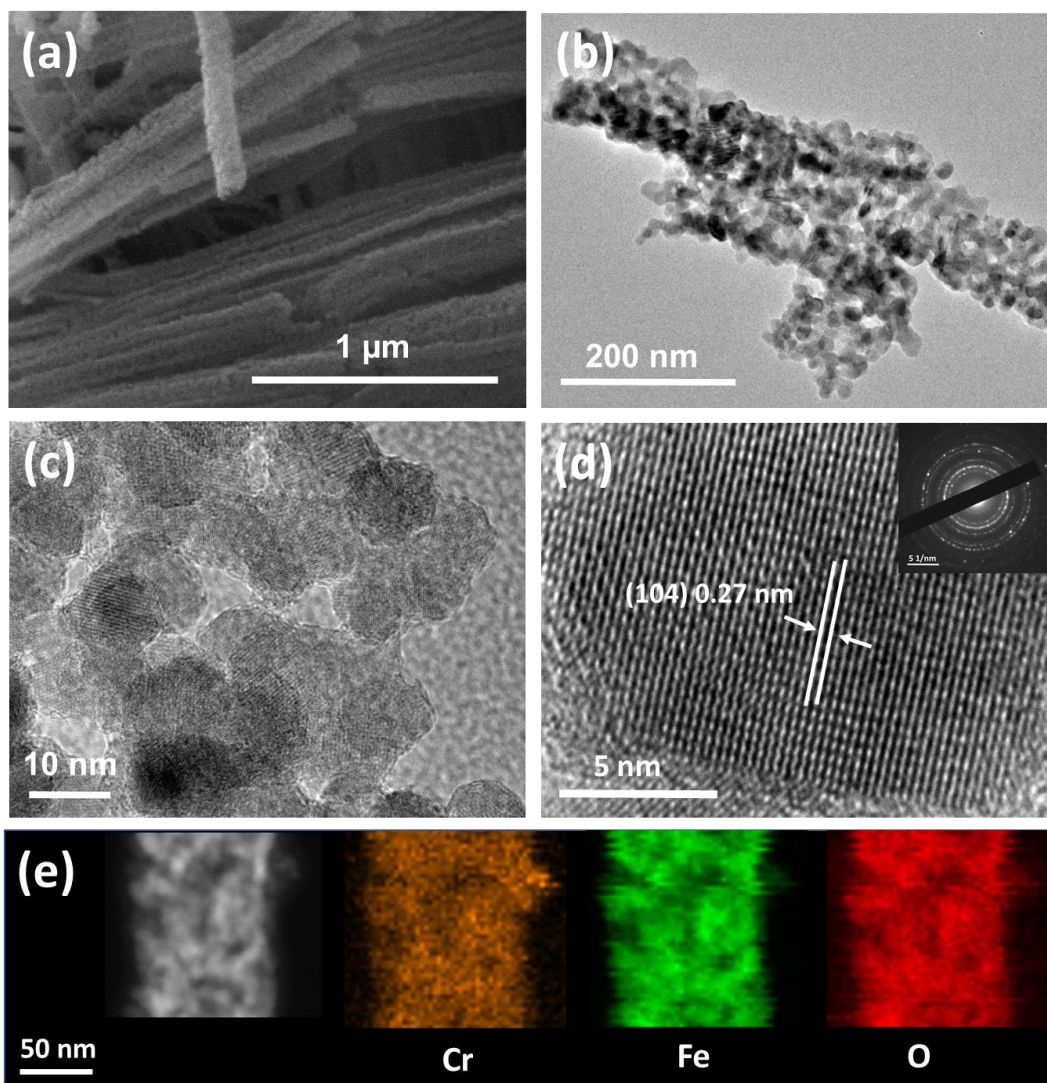


Figure 5.1 (a) SEM image, (b)-(d) TEM images (at different magnifications) and SAED pattern (inset) and (e) elemental mapping (Cr (orange), Fe (green), O (red)) of CrFeO₃ nanowires

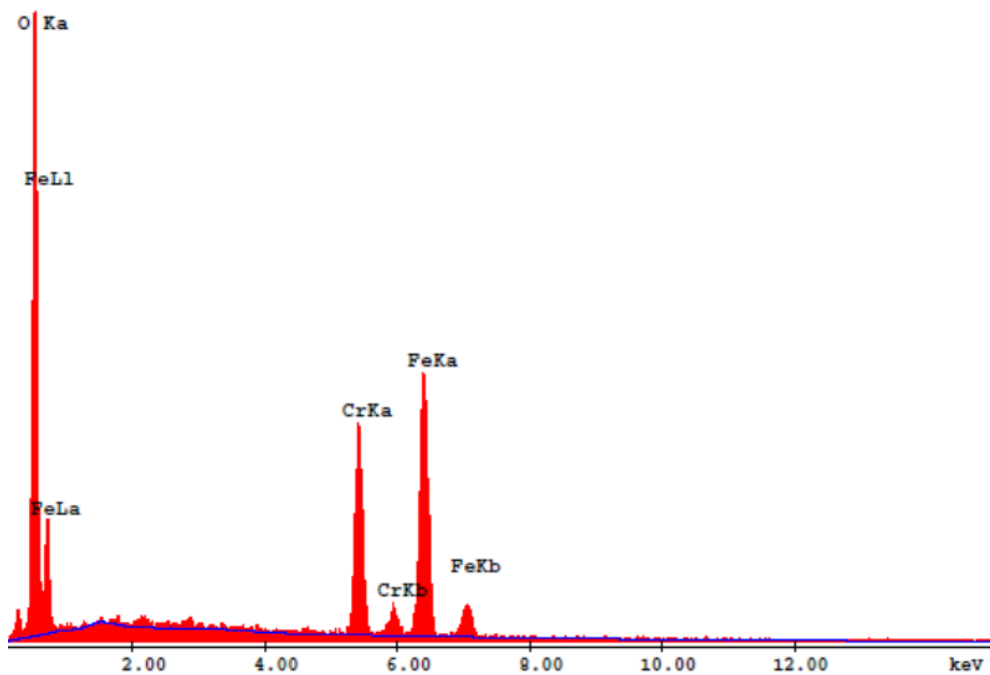


Figure 5.2 EDX spectra of CrFeO₃ nanowires

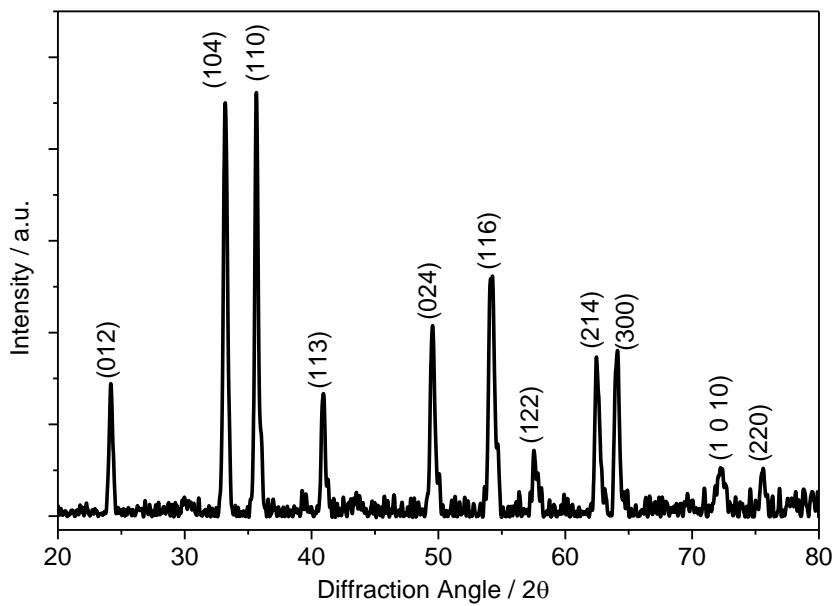
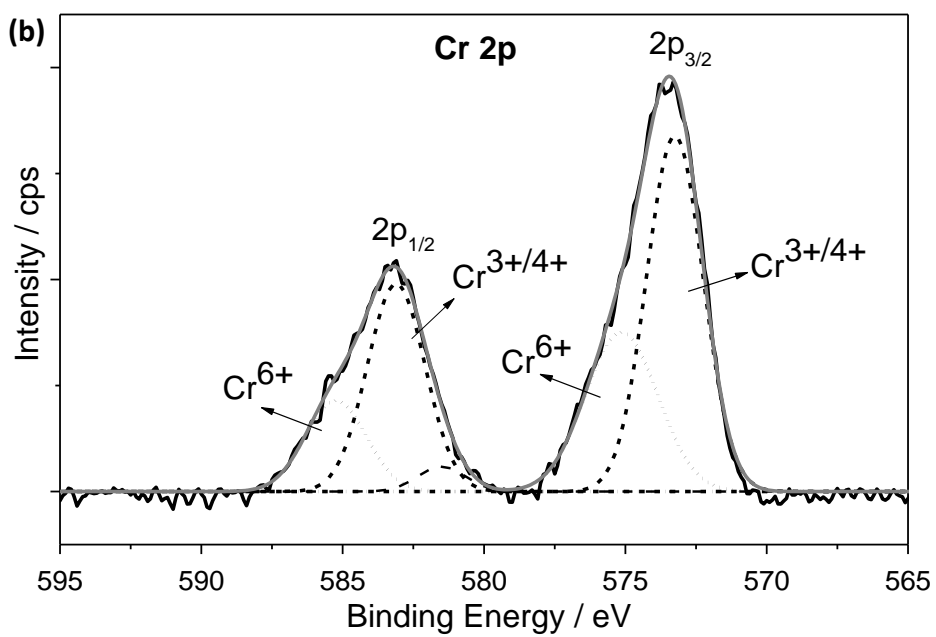
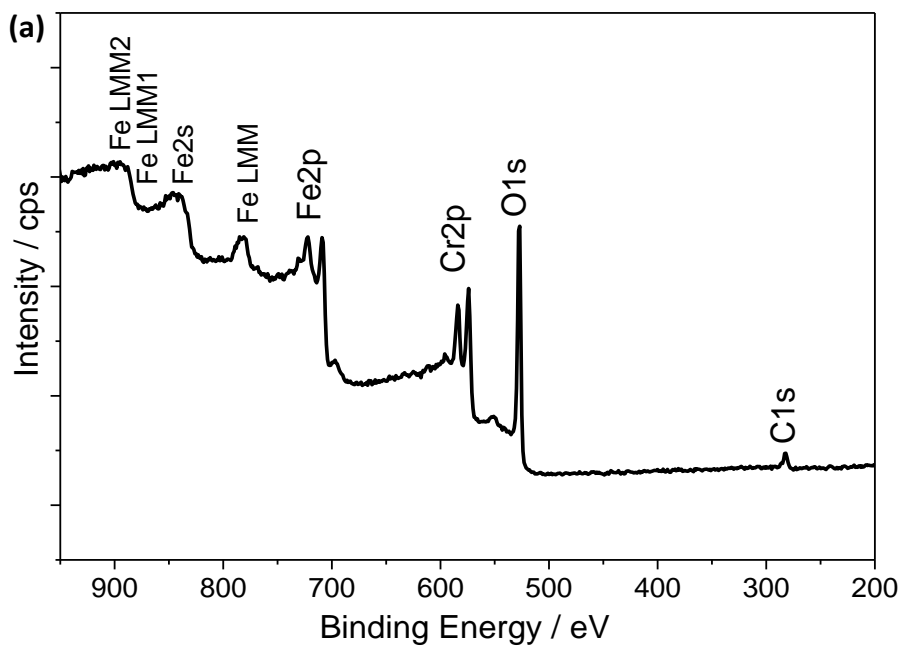


Figure 5.3 XRD Pattern of CrFeO₃ nanowires (JCPDS card no: 01-075-9861)

XRD pattern of CrFeO₃ nanowires is shown in Figure 5.3. The peaks observed at 2θ values of 24.3°, 33.3°, 35.8°, 41.0°, 49.6°, 54.2°, 57.8°, 62.5°, 64.1°, 72.0°, and 75.1° were assigned to the (012), (104), (110), (113), (024), (116), (122), (214), (300), (1 0 10), and (220) planes of CrFeO₃, respectively (JCPDS card no: 01-075-9861). CrFeO₃ nanowires contain all the observed diffraction peaks, so there was no detected impurity. The crystallite size of CrFeO₃ size was calculated by performing XRD peak analysis for the peak at 33.3° (104).⁴⁹ The analysis was carried out by using Debye-Scherrer equation.⁴² By the analysis, it was revealed that CrFeO₃ nanowires were formed by ca. 19.3 nm crystallites. The crystallite size was similar to the particle size measured by microscopy analyses.

The XPS spectrum of CrFeO₃ nanomaterials is demonstrated in Figure 5.4. Cr, Fe and O present in the synthesis product are shown in the survey spectra of the nanomaterials. Low quantity of carbon (C1s) at 282.4 eV which is used for calibration is the only contamination observed in the sample (Figure 5.4 a). Figure 5.3 b demonstrates the Cr 2p core-level spectrum of the synthesized nanomaterials. Corresponding peaks of Cr 2p_{1/2} and Cr 2p_{3/2} are observed at 586.1 eV and 576.5 eV, respectively. By the fitting process, each of these peaks was resolved to two Gaussian bands which are ascribed to Cr^{3+/4+} (583.0 eV and 573.4 eV) and Cr⁶⁺ (585.4 eV and 575.7 eV).^{50,51} It is difficult to observe the difference between the Cr³⁺ ion's peak and the one of Cr⁴⁺ since they have similar binding energies.^{50,51} Cr⁶⁺ ion's peak is not expected in perovskite (ABO₃) structure. It is the most conceivable reason for observing Cr⁶⁺ ions in the synthesized material is that oxidation of Cr⁴⁺ ions occurs on the nanomaterials' surface.⁵⁰ This result and the peak positions agree well with the ones of previously reported chromium materials.^{25,50,51} In the Figure 5.4 c, XPS spectrum of the Fe 2p is shown. In the spectrum, Fe 2p_{1/2} and Fe 2p_{3/2} peaks are observed at 721.8 eV and 708.0 eV, respectively. The fitting resulted two Gaussian bands under each of the Fe 2p peak. The presence of both Fe²⁺ (721.3 eV and 707.7 eV) and Fe³⁺ (723.4 eV and 709.6 eV) ions in the synthesized nanomaterial is proved by the comparison with the literature values.^{50,52-54} The O 1s spectrum given in Figure 5.4 d shows a peak at 527.5 eV. The peak is resolved two Gaussian bands by

the curve-fitting process. The band observed at 527.4 eV (I) and 529.5 eV (II) attribute the presence of metal-oxygen bonds and defect sites with low oxygen coordination, respectively.⁵⁵⁻⁵⁹



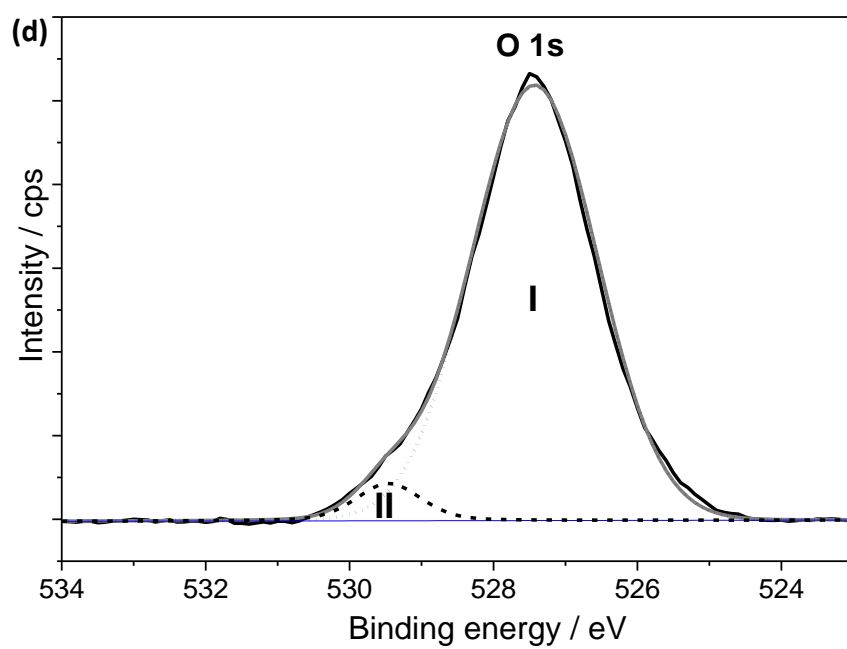
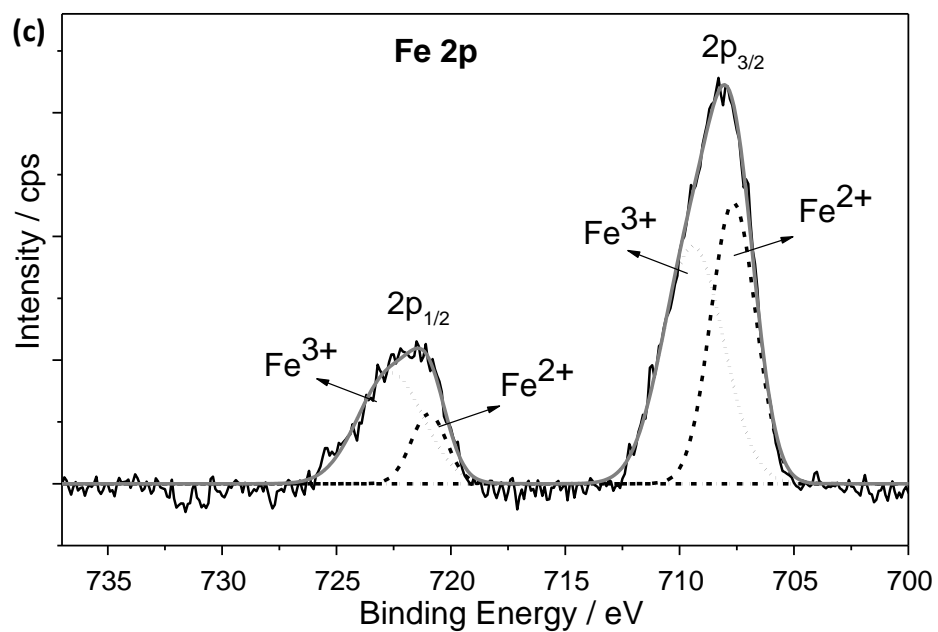


Figure 5.4 XPS (a) survey, (b) Cr 2p, (c) Fe 2p, (d) O1s spectra of CrFeO₃ nanowires

For the determination of the surface area and pore size of CrFeO₃ nanowires, BET analysis was performed. The specific surface area was measured as 61.9 m²/g. In addition, the presence of a hysteresis loop at relative pressure of ca. 0.4 in nitrogen adsorption-desorption isotherm suggest that CrFeO₃ nanowires have mesoporous structure with a pore size of 3.4 nm⁷ (Figure 5.5). To improve the interaction spot number, and thus to enhance catalytic performance of nanomaterial, the large surface area and porosity is crucial. The results of BET analysis revealed that CrFeO₃ nanowires have large surface area and porosity. Thus, the catalytic activity of CrFeO₃ nanomaterials is expected as well.

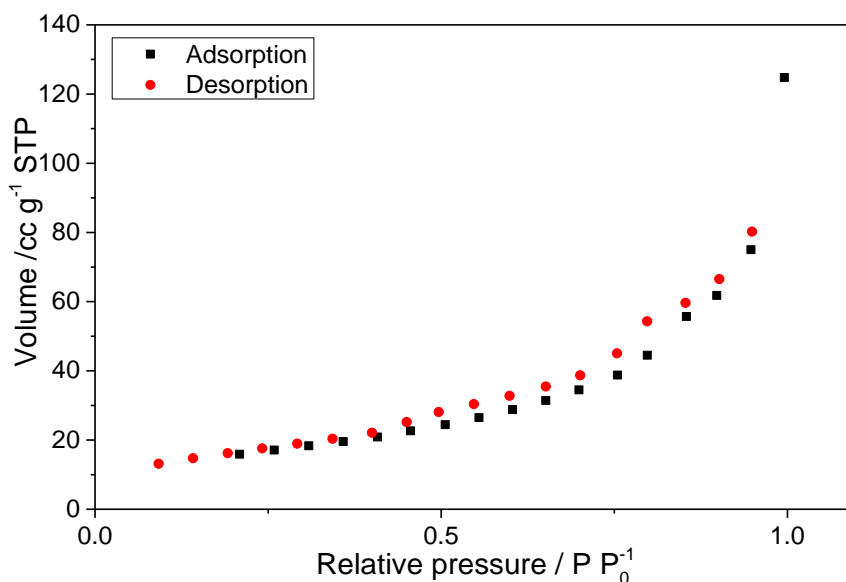


Figure 5.5 N₂ adsorption isotherm of CrFeO₃ nanowires

5.2 Electrocatalytic Performance of CrFeO₃ Nanowires

The electrocatalytic performance of FTO substrates modified with CrFeO₃ nanowires were investigated in oxygen evolution reaction (OER). The investigation was carried out in alkaline medium and at room temperature. The polarization curves of CrFeO₃ modified FTO electrodes (CrFeO₃-FTO) were studied to evaluate its electrocatalytic performance. Bare FTO and RuO₂ were also studied under the same

conditions to compare with CrFeO₃-FTO. These polarization curves are demonstrated in Figure 5.6. In the figure, it can be seen that after its modification with CrFeO₃ nanowires, electrocatalytic performance of bare FTO is significantly improved. The onset potential of CrFeO₃-FTO was determined as 1.63 V (vs RHE) from the polarization curve. In the research of Liu et al., RuO₂ showed very good activity with 1.34 V (vs RHE) onset potential and 190 mV overpotential at 10 mA cm⁻² current density (η_{10}). Also, Sun et al. and Gao et al. have reported similar electrochemical activities for RuO₂ nanomaterials. The onset potential of RuO₂ nanoparticles has been reported as 1.48 V (vs RHE) in both researches. However, there was a difference between overpotential values at 10 mA cm⁻² current density which were 325 mV⁴⁷ and 347 mV⁶⁰. In our study, the electrochemical activity of RuO₂ was found very similar to the reported ones. The results have been observed as 1.47 V (vs. RHE) onset potential and 346 mV overpotential at η_{10} . This value is slightly lower than CrFeO₃-FTO (1.63 V vs RHE). However, CrFeO₃-FTO has also comparable or even better onset potential than the ones of previously reported iron-based electrocatalysts. Some of the iron-based electrocatalyst from the literature are NiFe₂O₄ nanoparticles (NP) (1.70 V vs RHE), NiFe₂O₄ nanofiber (NF) (1.67 V vs RHE), MnFe₂O₄ NP (1.72 V vs RHE), MnFe₂O₄ NF (1.67 V vs RHE), CuFe₂O₄ NP (1.71 V vs RHE), CuFe₂O₄ NF (1.64 V vs RHE), CoFe₂O₄ NP (1.67 V vs RHE), CoFe₂O₄ NF (1.60 V vs RHE), CoFe₂O₄ (1.52 V vs RHE), Fe₂O₃ NP (1.67 V vs RHE), Fe₂O₃ NF (1.60 V vs RHE) and Fe₃O₄ (1.60 V vs RHE).^{19,27,31,61,62}

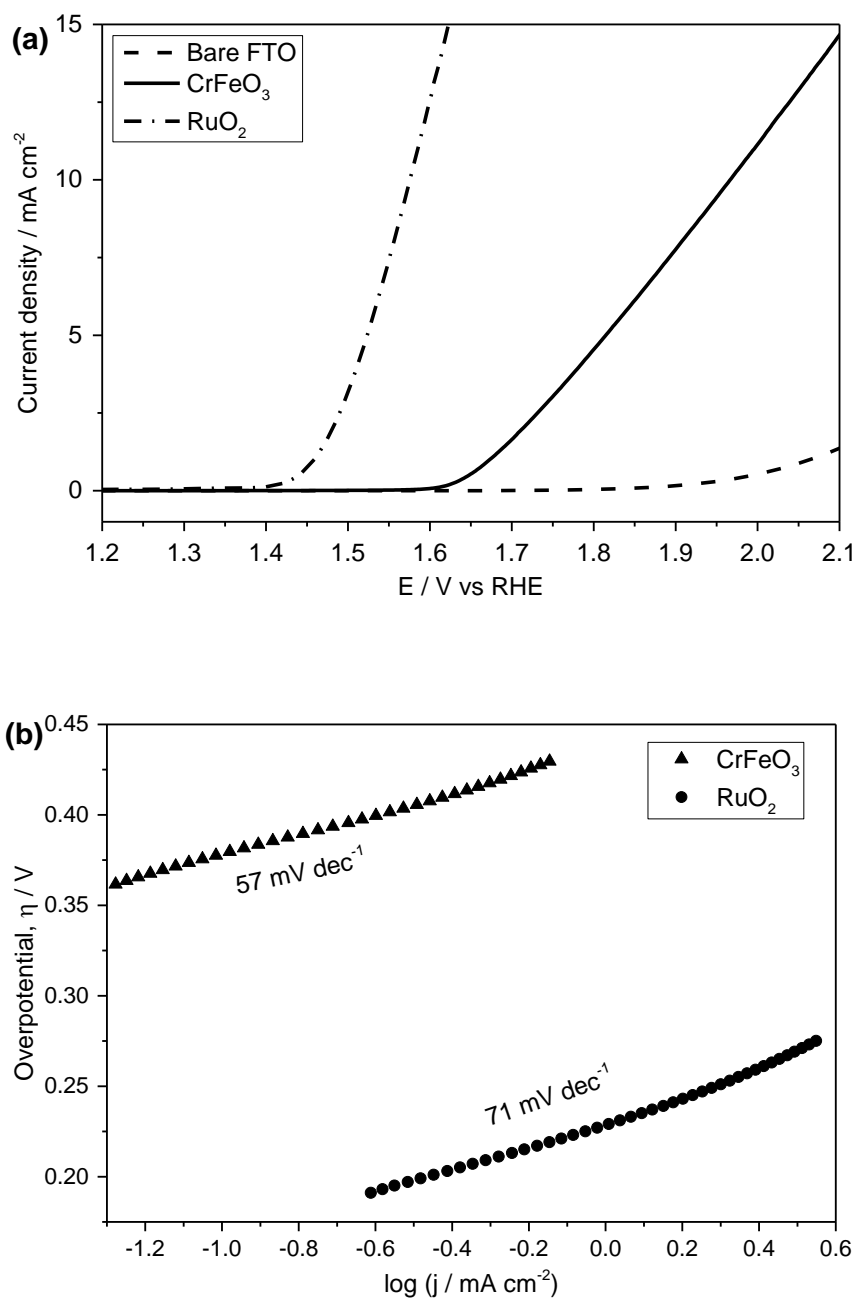


Figure 5.6 (a) Polarization curves of bare FTO, CrFeO₃ nanowires and RuO₂ in 0.1 M KOH at a scan rate of 5 mV s⁻¹ (b) Tafel slope of CrFeO₃ and RuO₂

To evaluate electrochemical activity of CrFeO₃ nanowires, overpotentials required to drive anodic current densities of 5 mA cm² (η_5) and 10 mA cm² (η_{10}) were also

used. CrFeO₃-FTO requires overpotentials of 584 mV (η_5) and 737 mV (η_{10}) to reach 5 mA cm⁻² and 10 mA cm⁻² current densities, respectively. The results obtained from CrFeO₃-FTO, and for comparison, some recently reported catalysts' performances are listed in Table 5.1.

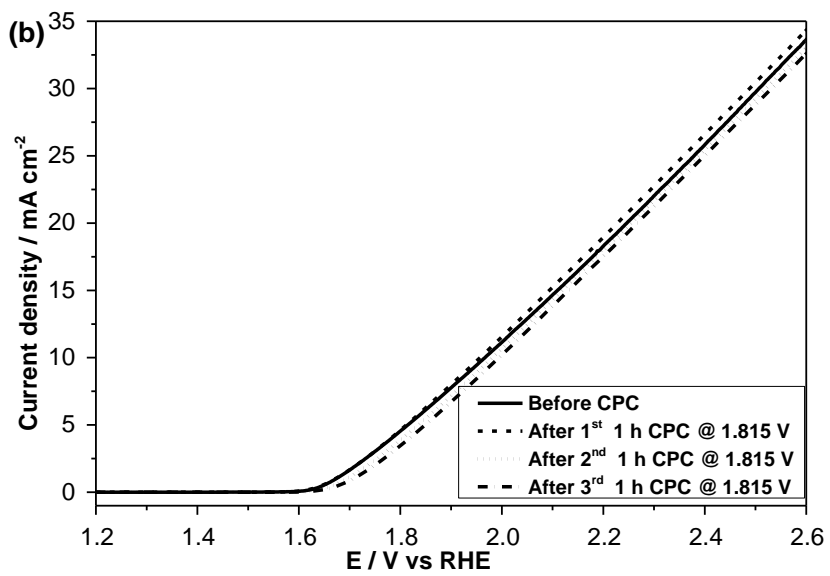
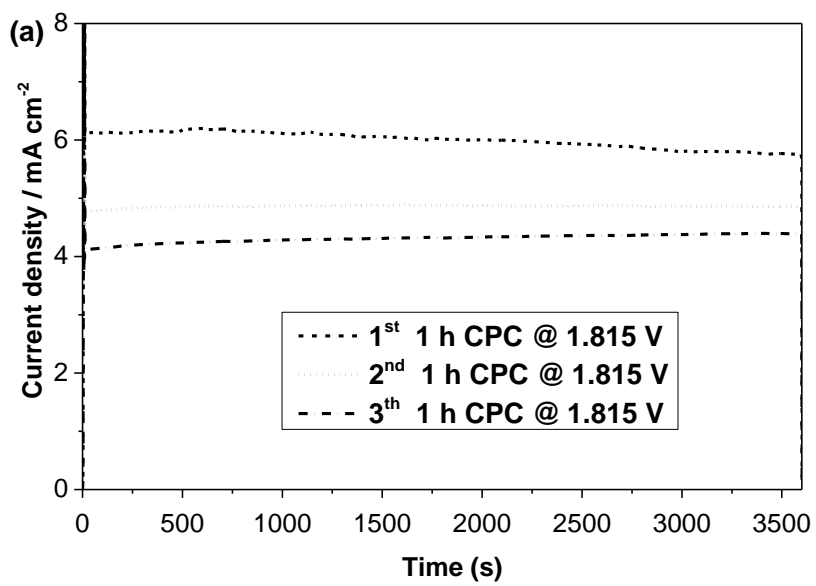
Table 5.1 Summary of some recently reported representative OER electrocatalysts in alkaline medium together with the data obtained for CrFeO₃ nanowires

| | Onset (RHE) | η (@10 mA/cm ²) | Tafel slope (mV/dec) | Medium | REF |
|-------------------------------------|-------------|----------------------------------|----------------------|-----------|---------------|
| CrFeO ₃ | 1.63 | 737 | 57 | 0.1 M KOH | This work |
| RuO ₂ | 1.47 | 346 | 71 | 0.1 M KOH | This work |
| CoFe ₂ O ₄ NP | 1.67 | - | 223.27 | 0.1 M KOH | ¹⁹ |
| CoFe ₂ O ₄ NF | 1.60 | - | 93.97 | 0.1 M KOH | ¹⁹ |
| NiFe ₂ O ₄ NP | 1.70 | - | 243.68 | 0.1 M KOH | ¹⁹ |
| NiFe ₂ O ₄ NF | 1.67 | - | 98.22 | 0.1 M KOH | ¹⁹ |
| MnFe ₂ O ₄ NP | 1.72 | - | 249.16 | 0.1 M KOH | ¹⁹ |
| MnFe ₂ O ₄ NF | 1.67 | - | 113.62 | 0.1 M KOH | ¹⁹ |
| CuFe ₂ O ₄ NP | 1.71 | - | 237.32 | 0.1 M KOH | ¹⁹ |
| CuFe ₂ O ₄ NF | 1.64 | - | 93.97 | 0.1 M KOH | ¹⁹ |
| NiFe ₂ O ₄ | ~1.55 | 370 | 44 | 1.0 M KOH | ² |
| CoFe ₂ O ₄ | ~1.52 | 333 | 47 | 1.0 M KOH | ⁶² |
| Fe ₃ O ₄ | ~1.6 | 470 | 143 | 1.0 M KOH | ²⁷ |
| Fe ₂ O ₃ NP | 1.79 | - | 285.59 | 0.1 M KOH | ¹⁹ |
| Fe ₂ O ₃ NF | 1.71 | - | 148.84 | 0.1 M KOH | ¹⁹ |

OER kinetics of CrFeO₃ nanowires were examined by fitting Tafel slope. In order to find Tafel slope, Tafel equation ($\eta = a + b \cdot \log(j)$, where η : overpotential, a: intercept giving the exchange current density j_0 , and b: Tafel slope) was used⁶³. In Figure 5.6 b, the Tafel slope of CrFeO₃-FTO and RuO₂ are given as 57 mV dec⁻¹ and 71 mV.dec⁻¹. Tafel slope of RuO₂ is similar to the recently reported values (i.e. 69 mV.dec⁻¹⁷, 70 mV.dec⁻¹⁶¹, 90 mV.dec⁻¹⁶⁰). As seen from Table 5.1, The Tafel slope of CrFeO₃ is comparable or smaller than that of RuO₂ and the ones of iron-based electrocatalysts such as NiFe₂O₄ NP (243.68 mV dec⁻¹), NiFe₂O₄ NF (98.22 mV dec⁻¹), MnFe₂O₄ NP (249.16 mV dec⁻¹), MnFe₂O₄ NF (113.62 mV dec⁻¹), CuFe₂O₄ NP (237.32 mV.dec⁻¹), CuFe₂O₄ NF (93.97 mV.dec⁻¹), CoFe₂O₄ (82.15 mV.dec⁻¹), Fe₂O₃ NP (285.59 mV.dec⁻¹), Fe₂O₃ NF (148.84 mV.dec⁻¹) and Fe₃O₄ (143 mV.dec⁻¹)^{19,27}. It can be said that OER kinetic of CrFeO₃ is faster than most of the other iron-based catalysts and RuO₂.

To enhance the catalytic performance evaluation of synthesized nanomaterial, the turnover frequency (TOF) value of modified electrode was also calculated. The TOF value of CrFeO₃-FTO was found as $2.2 \times 10^{-3} \text{ s}^{-1}$ at an overpotential of 737 mV. At the same overpotential, it was found as $4.1 \times 10^{-2} \text{ s}^{-1}$ for RuO₂.

To evaluate the stability of electrocatalyst during OER is very important. Therefore, the catalytic stability of CrFeO₃-FTO was also carried out in alkaline medium. In this investigation, constant potential electrolysis was performed at an overpotential of 585 mV (vs RHE) for 3 h. Polarization curves, which were recorded before and after the electrolysis are shown in Figure 5.7 a-d. Onset potentials and overpotential value equalled to current density of 10 mA cm⁻² were slightly increased from 1.63 V to 1.66 V vs RHE and from 737 mV to 765 mV, respectively. However, as seen in Figure 5.7 d, there is nearly no change in onset potentials and overpotential values upon further constant potential electrolysis at 1.97 V ($\eta=740$ mV). The obtained data were summarized in Table 5.2.



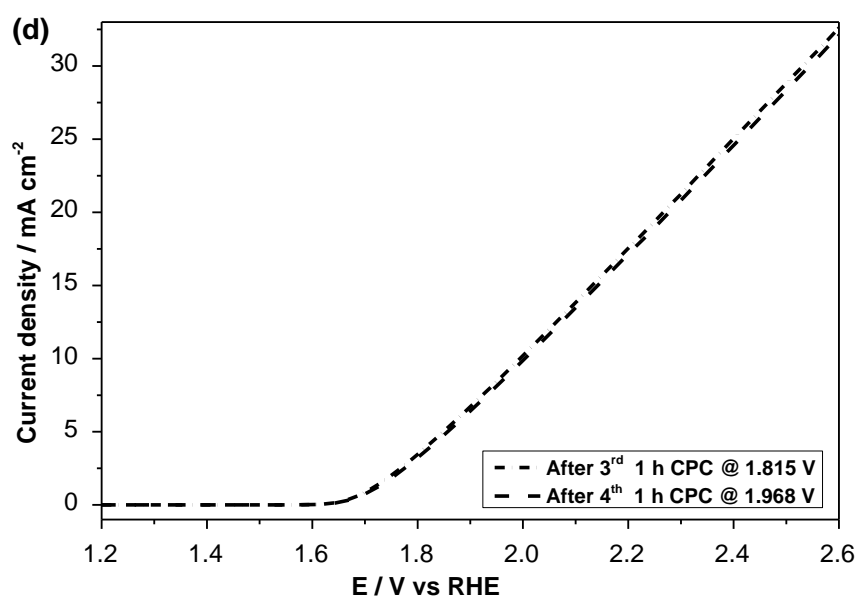
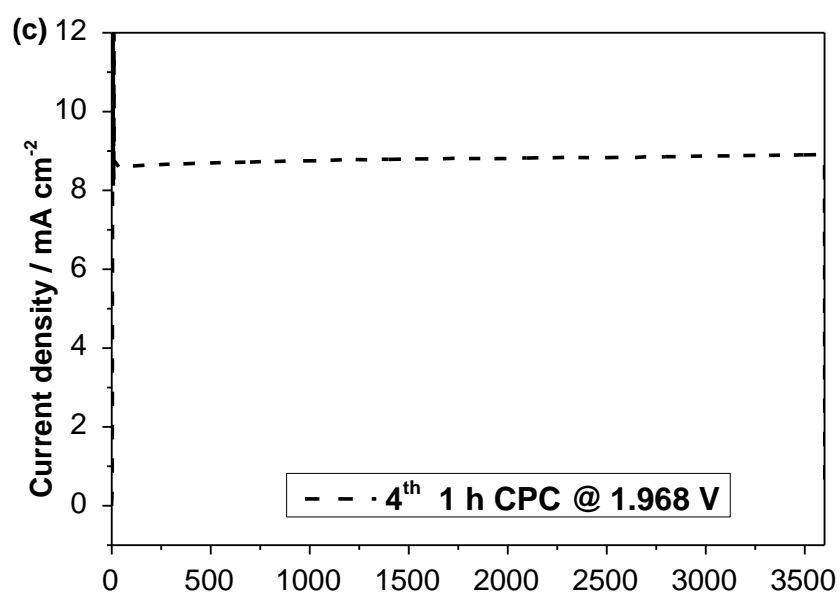


Figure 5.7 Current density changes during controlled potential electrolysis in 0.1 M KOH and Polarization curves of CrFeO₃ nanowires obtained before and after electrolysis at overpotential corresponding to initial current density of (a)-(b) $j = 5$ mA cm⁻² and (c)-(d) $j = 10$ mA cm⁻²

Table 5.2 Change in the onset potential and overpotential (at 10 mA cm⁻²) of CrFeO₃ nanowires after constant potential electrolysis

| | Onset (RHE) | η (@10 mA/cm²) |
|-------------------------|------------------------|----------------------------------|
| Before CPC | 1.63 | 737 |
| After 3 h CPC @ 1.815 V | 1.66 | 765 |
| After 1 h CPC @ 1.968 V | 1.66 | 773 |

EIS was performed at several overpotentials to examine the electrocatalytic performance of CrFeO₃-FTO. In Figure 5.8, The Nyquist plots of CrFeO₃-FTO comprise small and large semicircles in the high and low-frequency region, respectively. By using the electrical equivalent circuit diagram, the model of the data which fit to CPE was determined (Figure 5.8 inset). In this model, R_u and R_p correspond to solution resistance and charge transfer resistance (R_{ct}), respectively. As specific overpotential increased, decrease in the semicircles` diameter was observed. The result of this observation is that there is an increase in charge transfer kinetics during the OER process because of the decrease in the charge transfer resistance.

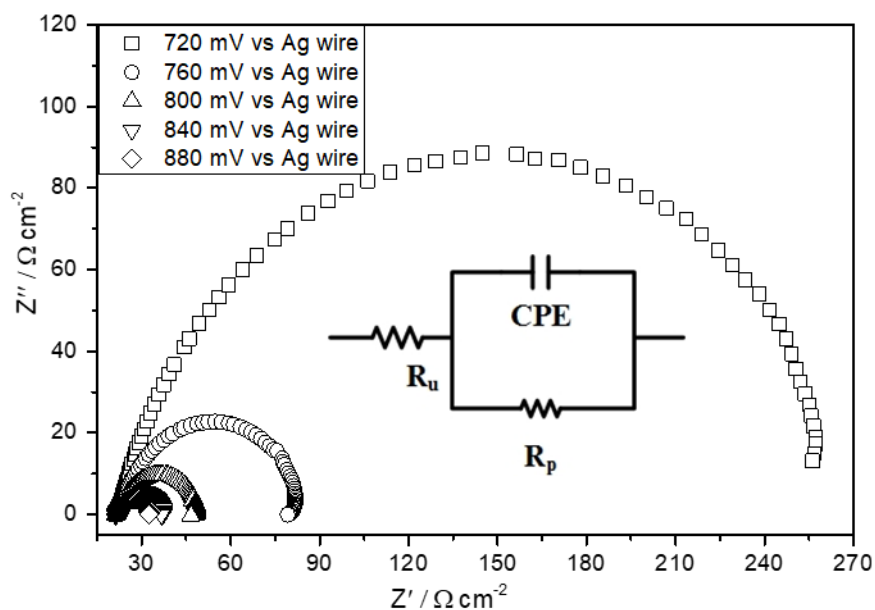


Figure 5.8 Nyquist plot for the CrFeO₃ nanowires modified FTO electrodes at different overpotentials

For the further evaluation of OER activity of CrFeO₃ nanowires, the volume of O₂ gas evolved from the electrolysis of water was also tested. The Hoffman electrolysis apparatus was used to find out the volume of O₂ gas during the electrolysis with the CrFeO₃ nanowires modified FTO electrode. The released O₂ amount (in mL) was detected for 3600 s at constant current of 5 mA and room temperature (Figure 5.9). After the transfer of 18 C of charge, the Faradaic yield of CrFeO₃-FTO for O₂ production was measured as >80 %. Since the amount of O₂ evolved and the theoretical yield are close to each other, it can be said that CrFeO₃ nanowires are very promising electrocatalyst for OER.

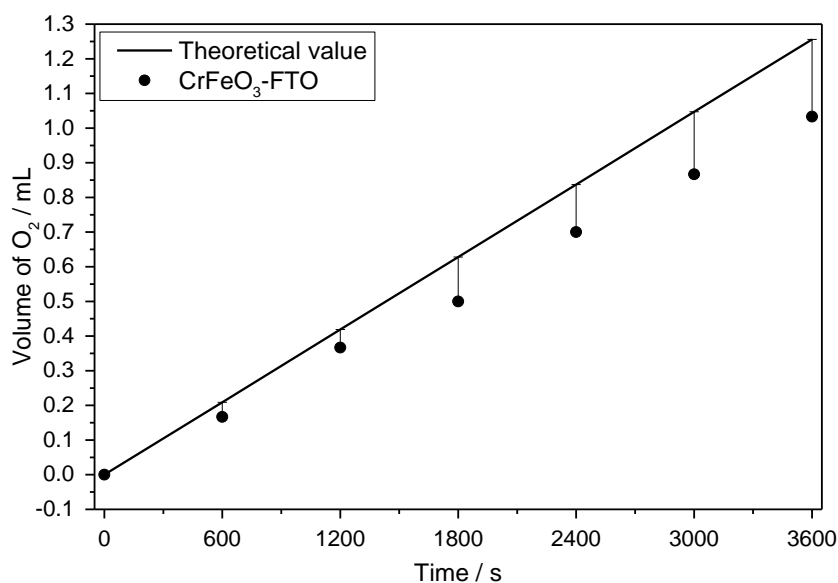


Figure 5.9 Plot for change in the volume of O₂ during the OER using the CrFeO₃-FTO in 0.1 M KOH

The catalytic performance of CrFeO₃ nanowires can be associated with both chemical and morphological properties of CrFeO₃ nanomaterials. In general, one of the most important quality of a good catalyst is the high surface area of both reactants and reaction intermediates. Small nanocrystallites of CrFeO₃ assemble, and then form one-dimensional nanowire. By assembling, the overall surface area of synthesized nanomaterial is expected to increase, and therefore, more exposed active sites for catalysis can be obtained. Thus, improvement electrical conductivity, charge transfer, and electrocatalytic water oxidation can be achieved. Another important parameter of a good catalyst is the presence of oxygen deficient sites in the structure. It has been reported that as H₂O molecule adsorb more to the oxygen deficient sites catalytic performance is enhanced.^{8,64,65} XPS O1s core level spectra prove that low oxygen coordination sites exist in the synthesized nanowires. In addition, the synergic relation between Cr and Fe in metal oxide structure could increase charge transfer in the material, and therefore, the electrocatalytic water oxidation reaction can improve.²⁴ All these investigations demonstrate that CrFeO₃ nanowires have a great potential as a catalyst not only for OER but also various other catalytic reactions.

CHAPTER 6

CONCLUSION

In this thesis study, the aim was to synthesize Cr-Fe-based bimetallic oxide nanoparticles to be used as electrocatalyst for water oxidation reaction. The synthesis was carried out by simple and low-cost hydrothermal methods in which NTA was used as a surface directing agent. The characterization of synthesized nanomaterials was performed via SEM, TEM, EDX-mapping, XRD, XPS and BET. After whole characterizations of the synthesized nanomaterial, CrFeO₃ nanowires, assembled by ca. 14 nm nanoparticles, were produced with BET surface area of 61.9 m²/g and pore size of 3.4 nm.

Electrocatalytic performances of CrFeO₃ nanowires as electrocatalyst were also tested in alkaline medium at room temperature. The results showed that CrFeO₃ nanowires modified FTO had 1.63 V vs RHE onset potential and 737 mV overpotential at 10 mA cm⁻² current density. Additionally, Tafel slope of the synthesized nanomaterial was determined as 57 mV dec⁻¹. The result was comparable to that of RuO₂ and better than some of the other iron based electrocatalysts.

In order to explore the durability of the synthesized nanocatalysts, controlled potential coulometry was performed for 3 hours. Onset potential and overpotential of CrFeO₃ nanowires were slightly increased from 1.63 to 1.66 V vs RHE and from 737 to 765 mV at 10 mA cm⁻² current density, respectively. After the durability test, good stability of CrFeO₃ nanowires during constant potential electrolysis was observed.

To conclude, CrFeO₃ nanowires can be considered as a new and very promising electrocatalyst since the nanomaterial can be easily synthesized and consist of earth-abundant, affordable metals for water oxidation reaction.

For further research, electrocatalytic performance of CrFeO₃ nanowires in hydrogen evolution reaction (HER), oxygen reduction reaction (ORR), metal air batteries or supercapacitors can be studied.

REFERENCES

1. Suen, N. T. *et al.* Electrocatalysis for the oxygen evolution reaction: Recent development and future perspectives. *Chem. Soc. Rev.* **46**, 337–365 (2017).
2. Liu, G., Wang, K., Gao, X., He, D. & Li, J. Fabrication of mesoporous NiFe₂O₄ nanorods as efficient oxygen evolution catalyst for water splitting. *Electrochim. Acta* **211**, 871–878 (2016).
3. Landon, J. *et al.* Spectroscopic Characterization of Mixed Fe–Ni Oxide Electrocatalysts for the Oxygen Evolution Reaction in Alkaline Electrolytes. *ACS Catal.* **2**, 1793–1801 (2012).
4. Liu, J. *et al.* Hierarchical nitrogen-enriched porous carbon materials derived from Schiff-base networks supported FeCo₂O₄ nanoparticles for efficient water oxidation. *Int. J. Hydrogen Energy* **42**, 10802–10812 (2017).
5. Liu, W. *et al.* NiCo₂O₄ ultrathin nanosheets with oxygen vacancies as bifunctional electrocatalysts for Zn-air battery. *Appl. Surf. Sci.* **478**, 552–559 (2019).
6. Grzelczak, M. *et al.* Electro- and Photochemical Water Oxidation on Ligand-free Co₃O₄ Nanoparticles with Tunable Sizes. *ACS Catal.* **3**, 383–388 (2013).
7. Sun, C. *et al.* Nanowires assembled from MnCo₂O₄@C nanoparticles for water splitting and all-solid-state supercapacitor. *Nano Res.* **9**, 1300–1309 (2016).

8. Zhao, Q., Yan, Z., Chen, C. & Chen, J. Spinels: Controlled Preparation, Oxygen Reduction/Evolution Reaction Application, and Beyond. *Chem. Rev.* **117**, 10121–10211 (2017).
9. Ekebas, E., Cetin, A., Önal, A. M. & Nalbant Esenturk, E. Magnesium substituted cobalt spinel nanostructures for electrocatalytic water oxidation. *J. Appl. Electrochem.* **49**, 315–325 (2019).
10. Kocabas, S., Cetin, A., Önal, A. M. & Esenturk, E. N. Chromium substituted iron oxide nanowires as affordable electrocatalysts for oxygen evolution reaction. *J. Nanoparticle Res.* **21**, 143 (2019).
11. Cetin, A., Önal, A. M. & Esenturk, E. N. Nanowires assembled from iron manganite nanoparticles: Synthesis, characterization, and investigation of electrocatalytic properties for water oxidation reaction. *J. Mater. Res.* (2019) doi:10.1557/jmr.2019.215.
12. Cetin, A. & Esenturk, E. N. Hierarchical nanowire and nanoplate-assembled NiCo₂O₄–NiO biphasic microspheres as effective electrocatalysts for oxygen evolution reaction. *Mater. Today Chem.* **14**, 100215 (2019).
13. Aksoy, I., Cetin, A. & Esenturk, E. N. Hierarchical microspheres of Co₂CrO₄ nanoplates for electrocatalytic water oxidation. *J. Nanoparticle Res.* **22**, (2020).
14. BANERJEE, A. *et al.* Catalytic decomposition of sulfuric acid on mixed Cr/Fe oxide samples and its application in sulfur–iodine cycle for hydrogen production. *Int. J. Hydrogen Energy* **33**, 319–326 (2008).

15. Freire, F. N. A. *et al.* Structural studies of a new electroceramic composite: Pb(Fe_{0.5}Nb_{0.5})O₃ (PFN)-Cr_{0.75}Fe_{1.25}O₃(CRFO). *J. Mater. Sci.* **43**, 75–82 (2008).
16. Rocha, H. H. B. *et al.* Structural properties study of the magneto-dielectric composite: Cr_{0.75}Fe_{1.25}O₃ (CRFO):Fe_{0.5}Cu_{0.75}Ti_{0.75}O₃(FCTO). *J. Alloys Compd.* **481**, 438–445 (2009).
17. de Araujo, J. C. S. *et al.* Dehydrogenation of ethylbenzene with CO₂ to produce styrene over Fe-containing ceramic composites. *Appl. Catal. A Gen.* **377**, 55–63 (2010).
18. Ozkendir, O. M. Electronic and crystal structure analysis of the FeCrO₃ oxide. *J. Electron Spectros. Relat. Phenomena* **191**, 54–59 (2013).
19. Li, M. *et al.* Facile synthesis of electrospun MFe₂O₄ (M = Co, Ni, Cu, Mn) spinel nanofibers with excellent electrocatalytic properties for oxygen evolution and hydrogen peroxide reduction. *Nanoscale* **7**, 8920–8930 (2015).
20. Elmaci, G., Frey, C. E., Kurz, P. & Zümreoğlu-Karan, B. Water Oxidation Catalysis by Birnessite@Iron Oxide Core–Shell Nanocomposites. *Inorg. Chem.* **54**, 2734–2741 (2015).
21. Yan, W. *et al.* One-pot synthesis of monodispersed porous CoFe₂O₄ nanospheres on graphene as an efficient electrocatalyst for oxygen reduction and evolution reactions. *RSC Adv.* **6**, 307–313 (2015).
22. Elmaci, G., Frey, C. E., Kurz, P. & Zümreoğlu-Karan, B. Water oxidation

- catalysis by using nano-manganese ferrite supported 1D-(tunnelled), 2D-(layered) and 3D-(spinel) manganese oxides. *J. Mater. Chem. A* **4**, 8812–8821 (2016).
23. Liu, G., Gao, X., Wang, K., He, D. & Li, J. Uniformly mesoporous NiO/NiFe₂O₄ biphasic nanorods as efficient oxygen evolving catalyst for water splitting. *Int. J. Hydrogen Energy* **41**, 17976–17986 (2016).
 24. Kanazawa, T. & Maeda, K. Chromium-substituted hematite powder as a catalytic material for photochemical and electrochemical water oxidation. *Catal. Sci. Technol.* **7**, 2940–2946 (2017).
 25. Chambers, S. A. *et al.* Electronic and Optical Properties of a Semiconducting Spinel (Fe₂CrO₄). *Adv. Funct. Mater.* **27**, 1605040 (2017).
 26. Bian, L. *et al.* Enhanced Photovoltage Response of Hematite-X-Ferrite Interfaces (X = Cr, Mn, Co, or Ni). *Nanoscale Res. Lett.* **12**, 136 (2017).
 27. Xie, Y., Wang, X., Tang, K., Li, Q. & Yan, C. Blending Fe₃O₄ into a Ni/NiO composite for efficient and stable bifunctional electrocatalyst. *Electrochim. Acta* **264**, 225–232 (2018).
 28. Fang, Z., Hao, Z., Dong, Q. & Cui, Y. Bimetallic NiFe₂O₄ synthesized via confined carburization in NiFe-MOFs for efficient oxygen evolution reaction. *J. Nanoparticle Res.* **20**, 106 (2018).
 29. Sun, S., Zhou, Z., Zhang, L. & Tang, R. Oxidation behavior and Stress Corrosion Cracking Susceptibility of Fe₂₇Ni₁₆Cr_{3.5}Al based AFA Alloy in

- Supercritical Water. *Mater. Res. Express* **5**, 066525 (2018).
30. Jin, Z., Li, P., Jin, Y. & Xiao, D. Superficial-defect engineered nickel/iron oxide nanocrystals enable high-efficient flexible fiber battery. *Energy Storage Mater.* **13**, 160–167 (2018).
 31. Liu, Y., Niu, Z., Lu, Y., Zhang, L. & Yan, K. Facile synthesis of CuFe₂O₄ crystals efficient for water oxidation and H₂O₂ reduction. *J. Alloys Compd.* **735**, 654–659 (2018).
 32. Yuan, F., Cheng, X., Wang, M. & Ni, Y. Controlled synthesis of tubular ferrite MFe₂O₄ (M = Fe, Co, Ni) microstructures with efficiently electrocatalytic activity for water splitting. *Electrochim. Acta* **324**, 134883 (2019).
 33. Benhalima, C., Amari, S., Beldi, L. & Bouhafs, B. First-Principles Study of Ferromagnetism in Iron Chromite Spinels: FeCr₂O₄ and CrFe₂O₄. *SPIN* **09**, 1950014 (2019).
 34. Ghoneim, A. I., Matsuda, A. & Tan, W. K. Structural, Thermal and Electrochemical studies of Sm substituted CrFeO₃ Nano-Pervoskites. *J. Alloys Compd.* **870**, 159420 (2021).
 35. Mubasher *et al.* Multi-walled carbon nanotubes and chromium ferrites nanoparticles nanohybrids as anode materials for lithium-ion batteries. *J. Alloys Compd.* **872**, 159654 (2021).
 36. Fernández-García, M. & Rodríguez, J. A. Metal Oxide Nanoparticles. in *Encyclopedia of Inorganic and Bioinorganic Chemistry* (John Wiley &

- Sons, Ltd, 2011). doi:10.1002/9781119951438.eibc0331.
37. Chavali, M. S. & Nikolova, M. P. Metal oxide nanoparticles and their applications in nanotechnology. *SN Appl. Sci.* **1**, 1–30 (2019).
 38. Ashrit, P. Introduction to Transition Metal Oxides and Thin Films. in *Transition Metal Oxide Thin Film based Chromogenics and Devices* 13–72 (Elsevier, 2017). doi:10.1016/B978-0-08-101747-0.00002-7.
 39. Niederberger, M. & Pinna, N. *Metal Oxide Nanoparticles in Organic Solvents*. (Springer London, 2009). doi:10.1007/978-1-84882-671-7.
 40. Rao, D. C. K., Yadav, N. & Joshi, P. C. Cu–Co–O nano-catalysts as a burn rate modifier for composite solid propellants. *Def. Technol.* (2016) doi:10.1016/j.dt.2016.01.001.
 41. *Nanocatalysis Synthesis and Applications*. (John Wiley & Sons, Inc., 2013). doi:10.1002/9781118609811.
 42. Kumar, C. G., Pombala, S., Poornachandra, Y. & Agarwal, S. V. Synthesis, characterization, and applications of nanobiomaterials for antimicrobial therapy. in *Nanobiomaterials in Antimicrobial Therapy: Applications of Nanobiomaterials* (2016). doi:10.1016/B978-0-323-42864-4.00004-X.
 43. Faunce, T. *et al.* Artificial photosynthesis as a frontier technology for energy sustainability. *Energy Environ. Sci.* **6**, 1074 (2013).
 44. Bofill, R., García-Antón, J., Escriche, L. & Sala, X. Chemical, electrochemical and photochemical molecular water oxidation catalysts. *J.*

- Photochem. Photobiol. B Biol.* **152**, 71–81 (2015).
45. *Methods for Electrocatalysis*. (Springer International Publishing, 2020). doi:10.1007/978-3-030-27161-9.
 46. Demir, E., Akbayrak, S., Önal, A. M. & Özkar, S. Nanoceria-Supported Ruthenium(0) Nanoparticles: Highly Active and Stable Catalysts for Hydrogen Evolution from Water. *ACS Appl. Mater. Interfaces* **10**, 6299–6308 (2018).
 47. Sun, C. *et al.* Nanowires assembled from MnCo₂O₄@C nanoparticles for water splitting and all-solid-state supercapacitor. *Nano Res.* **9**, 1300–1309 (2016).
 48. Lee, S. Y. *et al.* Screen-Printed Calcium-Birnessite Electrodes for Water Oxidation at Neutral pH and an “Electrochemical Harriman Series”. *ChemSusChem* **7**, 3442–3451 (2014).
 49. Kim, D.-W., Rhee, K.-Y. & Park, S.-J. Synthesis of activated carbon nanotube/copper oxide composites and their electrochemical performance. *J. Alloys Compd.* **530**, 6–10 (2012).
 50. Xu, S. *et al.* Perovskite chromates cathode with resolved and anchored nickel nano-particles for direct high-temperature steam electrolysis. *J. Power Sources* **246**, 346–355 (2014).
 51. Yao, W., Duan, T., Li, Y., Yang, L. & Xie, K. Perovskite chromate doped with titanium for direct carbon dioxide electrolysis. *New J. Chem.* **39**, 2956–2965 (2015).

52. Ding, J., Zhong, Q. & Zhang, S. Simultaneous removal of NOX and SO2 with H2O2 over Fe based catalysts at low temperature. *RSC Adv.* **4**, 5394 (2014).
53. Lobo, L. S. & Rubankumar, A. Investigation on structural and electrical properties of FeMnO3 synthesized by sol-gel method. *Ionics (Kiel)*. **25**, 1341–1350 (2019).
54. Pham, M.-H., Dinh, C.-T., Vuong, G.-T., Ta, N.-D. & Do, T.-O. Visible light induced hydrogen generation using a hollow photocatalyst with two cocatalysts separated on two surface sides. *Phys. Chem. Chem. Phys.* **16**, 5937 (2014).
55. Guan, X. Morphology-tuned Synthesis of MgCo2O4 Arrays on Graphene Coated Nickel Foam for High-Rate Supercapacitor Electrode. *Int. J. Electrochem. Sci.* 2272–2285 (2018) doi:10.20964/2018.03.35.
56. Nagamuthu, S., Vijayakumar, S., Lee, S.-H. & Ryu, K.-S. Hybrid supercapacitor devices based on MnCo₂O₄ as the positive electrode and FeMn₂O₄ as the negative electrode. *Appl. Surf. Sci.* **390**, 202–208 (2016).
57. Li, G., Liu, X. & Bai, W. Fabrication of porous MgCo₂O₄ with rod-like morphology and its superb catalytic activity towards ammonium perchlorate thermal decomposition. *Mater. Res. Express* **5**, 035036 (2018).
58. Pukazhselvan, D. *et al.* Two step mechanochemical synthesis of Nb doped MgO rock salt nanoparticles and its application for hydrogen storage in MgH₂. *Int. J. Hydrogen Energy* **41**, 11716–11722 (2016).

59. Silambarasan, M., Ramesh, P. S., Geetha, D. & Venkatachalam, V. A report on 1D MgCo₂O₄ with enhanced structural, morphological and electrochemical properties. *J. Mater. Sci. Mater. Electron.* **28**, 6880–6888 (2017).
60. Gao, M. *et al.* Efficient Water Oxidation Using Nanostructured α -Nickel-Hydroxide as an Electrocatalyst. *J. Am. Chem. Soc.* **136**, 7077–7084 (2014).
61. Liu, J. *et al.* Hierarchical nitrogen-enriched porous carbon materials derived from Schiff-base networks supported FeCo₂O₄ nanoparticles for efficient water oxidation. *Int. J. Hydrogen Energy* **42**, 10802–10812 (2017).
62. Yang, H. *et al.* Lateral-Size-Mediated Efficient Oxygen Evolution Reaction: Insights into the Atomically Thin Quantum Dot Structure of NiFe₂O₄. *ACS Catal.* **7**, 5557–5567 (2017).
63. Zhao, Y. *et al.* A study of photocatalytic, chemical, and electrocatalytic water oxidation on ACo₂O₄ (A=Ni, Cu, Zn) samples through doping different metal ions. *J. Catal.* **338**, 30–37 (2016).
64. Bao, J. *et al.* Ultrathin Spinel-Structured Nanosheets Rich in Oxygen Deficiencies for Enhanced Electrocatalytic Water Oxidation. *Angew. Chemie Int. Ed.* **54**, 7399–7404 (2015).
65. Cheng, F. *et al.* Enhancing Electrocatalytic Oxygen Reduction on MnO₂ with Vacancies. *Angew. Chemie Int. Ed.* **52**, 2474–2477 (2013).

APPENDICES

A. Characterizations of CrFeO₃ Nanowires at 550 °C Calcination Temperature

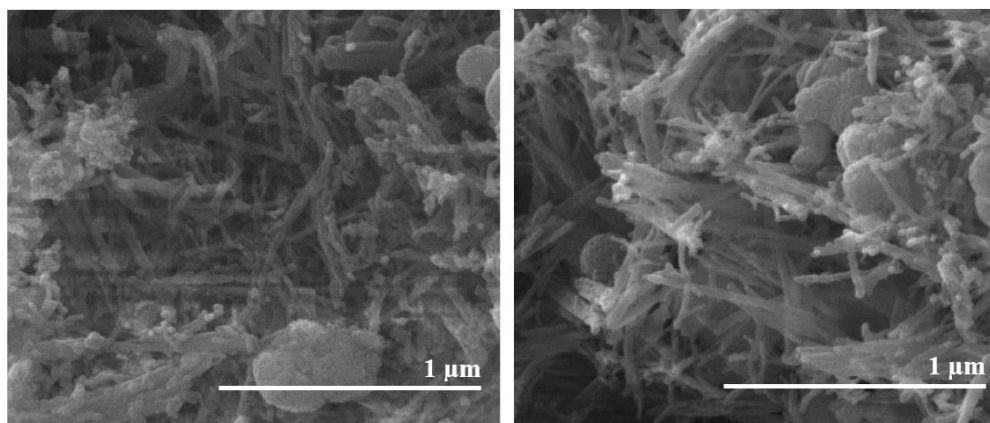


Figure A 1 SEM images of CrFeO₃ nanowires calcined at 550 °C temperature

B. Characterizations of CrFeO₃ Nanowires at 650 °C Calcination Temperature

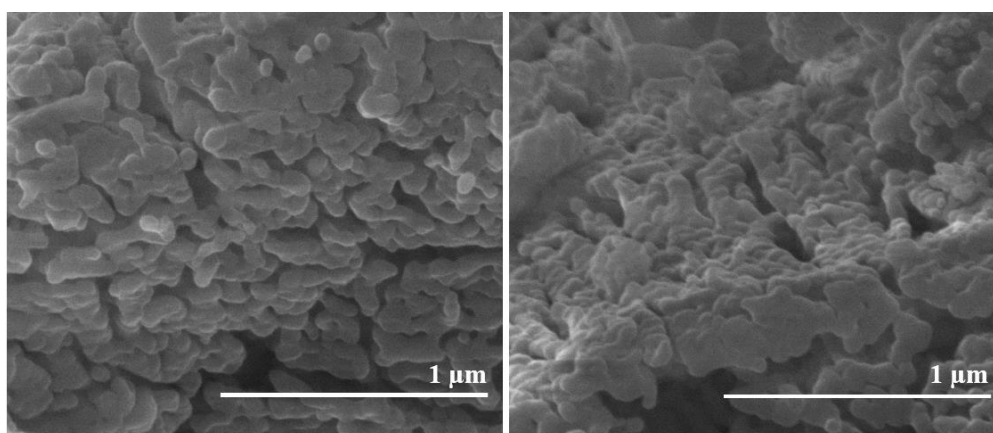


Figure B 1 SEM images of CrFeO₃ nanowires calcined at 650 °C temperature